AD-A264 241

TATION PAGE

	2. REPORT DATE	3. REPORT TYPE AND DATES COVERED
1. AGENCY USE ONLY (Leave blank)	December 1992	Technical Report

4. TITLE AND SUBTITLE

Cyclic Load Testing of Unreinforced Masonry Walls

5. FUNDING NUMBERS

DAAL03-87-K-0006

6. AUTHOR(S)

Daniel P. Abrams & Nirav Shah

7. PERFORMING ORGANIZATION NAME(S) AND ADDRESS(ES)

Advanced Construction Technology Center
University of Illinois at Urbana-Champaign
Department of Civil Engineering
205 N. Mathews Ave., MC - 250
Urbana, IL 61801

DTIC
ELECTE
MAY 06 1993
S E D

8. PERFORMING ORGANIZATION REPORT NUMBER

ACTC Document #92-26-10

9. SPONSORING/MONITORING AGENCY NAME(S) AND ADDRESS(ES)

U.S. Army Research Office
P.O. Box 12211
Triangle Park, NC 27709-2211

10. SPONSORING/MONITORING AGENCY REPORT NUMBER

ARO 24605.162-EG-UIR

11. SUPPLEMENTARY NOTES

12a. DISTRIBUTION/AVAILABILITY STATEMENT

Approved for public release; distribution unlimited.

12b. DISTRIBUTION CODE

13. ABSTRACT *(Maximum 200 words)*

The report presents results of three laboratory experiments done to investigate in-plane lateral strength and behavior of unreinforced masonry walls. The parameters of the experimental study were the length-to-height aspect ratio of the test walls and the level of vertical compressive stress. Wall specimens were newly constructed using reclaimed brick and a mortar representative of older construction. Measured strength and behavior of the test walls is correlated with each other, with computational models and with estimates based on nondestructive measurements.

Results of the experiments suggest that (a) an unreinforced masonry wall can resist more than twice the lateral force resulting in the first crack, (b) inelastic deformation capacity can be very large for walls that are cracked in both flexure and diagonal tension, (c) capacity for hysteretic energy dissipation can be large despite cracking, and (d) cyclic behavior can be represented in terms of behavior under monotonically increasing forces. These conclusions have an impact on the way that nondestructive measurements are extrapolated when diagnosing levels of safety for lateral strength of isolated walls as well as for complete building systems.

93 5 05 038

93-09745

14. SUBJECT TERMS

15. NUMBER OF PAGES

40

16. PRICE CODE

17. SECURITY CLASSIFICATION OF REPORT	18. SECURITY CLASSIFICATION OF THIS PAGE	19. SECURITY CLASSIFICATION OF ABSTRACT	20. LIMITATION OF ABSTRACT
UNCLASSIFIED	UNCLASSIFIED	UNCLASSIFIED	UL

Technical Report

This is a Technical Report, Document #92-26-10, for the Advanced Construction
Technology Center Project titled *NDE of Masonry Buildings*, Project #26. Professor
D.P. Abrams is the project investigator. The reproduction is provided for other
researchers, particularly those researchers in Army Laboratories interested in this
work.

Accesion For		
NTIS CRA&I		X
DTIC TAB		☐
Unannounced		☐
Justification		
By		
Distribution /		
Availability Codes		
Dist	Avail and / or Special	
A-1		

ABSTRACT

Cyclic Load Testing of Unreinforced Masonry Walls

by

Daniel P. Abrams and Nirav Shah
Department of Civil Engineering
University of Illinois at Urbana-Champaign

The report presents results of three laboratory experiments done to investigate in-plane lateral strength and behavior of unreinforced masonry walls. The parameters of the experimental study were the length-to-height aspect ratio of the test walls and the level of vertical compressive stress. Wall specimens were newly constructed using reclaimed brick and a mortar representative of older construction. Measured strength and behavior of the test walls is correlated with each other, with computational models and with estimates based on nondestructive measurements.

Results of the experiments suggest that (a) an unreinforced masonry wall can resist more than twice the lateral force resulting in the first crack, (b) inelastic deformation capacity can be very large for walls that are cracked in both flexure and diagonal tension, (c) capacity for hysteretic energy dissipation can be large despite cracking, and (d) cyclic behavior can be represented in terms of behavior under monotonically increasing forces. These conclusions have an impact on the way that nondestructive measurements are extrapolated when diagnosing levels of safety for lateral strength of isolated walls as well as for complete building systems.

TABLE OF CONTENTS

CHAPTER 1.
INTRODUCTION

1.1 Preface

Lateral strength of a building structure may need to be evaluated when the function of a building is redefined, when loadings are increased, when building code specifications are updated, when risk assessments for insurance purposes are to be made, or when the structure shows signs of deterioration. Buildings that have stood up for decades are well proven in terms of their capability to resist gravity loadings. However, their ability to resist lateral forces such as from earthquakes, winds, blasts or impacts may remain uncertain because extreme loadings seldom are realized, and the structural system cannot be given a true test. Despite the small probability associated with the occurrence of extreme lateral loadings, lateral strength of a building must be estimated and checked against anticipated demands. This creates a paradox for a structural engineer because he or she is forced to use analytical approaches that are sometimes left unproven.

When lateral strength of an unreinforced masonry building is to be evaluated, it is necessary to resort to simple and conservative assumptions regarding behavior of walls or piers resisting forces within their plane. Assumptions such as linear, uncracked behavior have to be employed since little is known about behavior after the formation of the first crack. For cases of alternating forces such as would occur when a building oscillates back and forth during an earthquake, very little is known about the interaction of cracks in the masonry under repeated and reversed loadings.

Common assumptions used today limit lateral strength of a system to the strength of its weakest element. The lateral load capacity may be limited to that force which is necessary to crack the first pier or wall. If it can be shown that an unreinforced wall or pier can resist lateral force after formation of the first crack with little or no loss of strength, then it may be assumed that adjacent elements will not be required to foster the lost load. In other words, lateral strength of the system may be assumed to be comprised of the combined strengths of all of its elements. If this one assumption of ductile behavior can be made, then estimates of system strength may be several times greater than those limited by the first crack of the weakest element. However, ductility of unreinforced masonry is still highly questionable because of the lack of experimental evidence on its true behavior when subjected to lateral forces.

Behavior of unreinforced walls or piers subjected to in-plane lateral forces has been found to be dominated by either flexure, shear or some combination of the two. Flexural behavior consists of cracking along horizontal bed joints usually at the base of an element where the moment is the largest. Flexural behavior is common for relatively tall elements with light amounts of vertical compressive stress. Shear behavior consists of diagonal cracking either through bricks and mortar joints for relatively weak bricks and strong mortars, or in a stair-stepped manner through the mortar head and bed joints for relatively strong bricks and weak mortars. Shear cracking may also consist of sliding along bed joints. Shear behavior is common for stocky elements with rela-

1

tively heavy amounts of vertical compressive stress. Combinations of flexure and shear behavior may exist for elements that first crack in flexure, then redistribute shear stress across a smaller uncracked portion, and subsequently crack in diagonal tension.

The purpose of the research reported herein is to investigate these three basic behavioral modes for in-plane shear resistance of unreinforced masonry walls. Laboratory test data is presented on three sample walls of different height-to-length aspect ratios. Unlike former studies, the focus of investigation is on behavior under lateral forces that reverse when they are repeated. This report summarizes the laboratory tests, and presents experimental data that supports the notion that unreinforced masonry walls or piers may indeed be considered as ductile elements in resisting lateral forces. The underlying message that the research results give is that the post-cracking behavior of an unreinforced masonry wall may be substantial. This implies that lateral strength of a building system may be estimated as the sum of its parts rather than be limited by the strength of its weakest element.

1.2 Research Objective and Scope

The objective of this research was to quantify force-deflection behavior of unreinforced masonry walls loaded within their plane. It was of particular interest to examine (a) strength and deformation capacity, (b) the influence of cracking on shear and normal stress distributions, and (c) the relation between actual strength and nondestructive estimates of strength.

The scope of the research included a study of lateral force behavior of unreinforced masonry walls dominated by flexure, shear or a combination of flexure and shear. Three walls were built and tested in the Newmark Civil Engineering Laboratory. These walls were intended to represent existing masonry structures built in the first half of this century. The walls were subjected to in-plane shear forces, which were cycled according to a predefined pattern. Nondestructive tests were done before testing to provide data on masonry shear strength for correlation studies with ultimate strengths.

1.3 Background Information

1.3.1 Previous Research

The research reported herein is a subsequent project to an earlier one done by Gary Epperson and reported on in Ref. 11. In the Epperson study a series of six unreinforced masonry walls were extracted from a building constructed in 1917, and transported to the Newmark Laboratory for testing. Lateral forces were applied within the plane of the test walls while vertical compressive stress was maintained constant for each wall. Though the test walls were only subjected to monotonically increasing forces, the tests did reveal that an URM wall can possess substantial life after initial cracking. Ultimate loads were from two to three times the strength at first cracking, and the walls could resist considerable lateral deformations before the ultimate limit state was reached. Because flexural cracks extended over half of the wall length, the effective shear zone was greatly reduced.

2

Weijia Xu (Ref. 6) developed an analytical model that determines distribution of shear stress as influenced by effects of flexural and shear cracking. This study showed with the use of analytical models, how shear stress is redistributed along the length of the wall once a crack has been formed. Though the masonry was considered elastic in compression, force–deflection behavior of a wall was represented in a nonlinear manner because of the progression of shear or flexural cracking. An index value quantifying the likelihood of shear sliding along a bed joint was defined as the ratio of applied shear stress to sliding resistance. Contour maps of the shear sliding index were drawn that depicted the zone of a wall that was most likely to have a shear sliding failure. A computer program and a set of tables were developed based on the analytical model for estimating lateral strength of cracked walls.

Abrams (Refs. 2 and 3) proposed a simple procedure for assessing lateral strength of masonry walls with little or no flexural tensile strength. The method relied on the redistribution of flexural stress after cracking, and limited lateral force to that resulting in a permissible value of toe compressive stress. Shear strength of the masonry was assumed to be effective across only the uncracked portion of masonry, and a reduction factor was proposed that accounts for the extent of flexural cracking.

1.3.2 Present Evaluation Requirements for Masonry Buildings

Although standards for evaluating lateral strength of masonry buildings is still evolving, there is one code that has emerged since the 1989 Loma Prieta Earthquake that has been used extensively in California. There is a Appendix to the Uniform Code for Building Conservation (UCBC) entitled *Seismic Strengthening Provisions for Unreinforced Masonry Bearing Wall Buildings* (Ref. 20) that prescribes how the lateral capacity of a wall should be estimated. An allowable value of shear stress, v_a, is given using the following equation :

$$v_a = 0.1v_t + 0.15\frac{P_D}{A} \qquad [1.1]$$

where: v_a = allowable shear stress for unreinforced masonry; v_t = mortar shear strength determined by in situ measurement (see discussion below); P_D = superimposed dead load; A = area of unreinforced masonry pier. The total shear strength of a wall is then determined by multiplying the allowable stress, v_a, by the gross area of a wall.

The assumption that shear stress is resisted across the entire gross section is appropriate if no flexural cracking occurs along the base of a wall. Whereas it is a safe practice to limit flexural tensile stress at the heel of a wall to an allowable value, past research has shown it to be a highly conservative practice. The post–cracking strength of a wall has been shown to be as much as three times larger than the pre–cracked strength. If post–cracking behavior is to be considered, a standard for strength evaluation should consider the wall aspect ratio *(L/h)* and the vertical compressive stress, σ_v. These two parameters will dictate the extent of flexural cracking, and thus the amount of effective shear area. At present, these two parameters are neglected.

The term v_t in Eq. 1.1 is determined from a nondestructive test known as the "in–place shear test" or in the testing methodology lingo as the "shove test" or the "push test." The method consists

3

of removing a single brick to create a void where a small hydraulic jack can be inserted. The brick adjacent to this void is the test brick which is sheared relative to its upper and lower mortar bed joints (the head joint on the opposite side of the adjacent brick is also removed). The stress, v_{to}, is determined by the following equation:

$$v_{to} = (V_{test} - P_{D+L})/A_b \qquad [1.2]$$

where V_{test} is the shear force measured with the in-place shear test; P_{D+L} is the estimated gravity force at the measurement location; and A_b is the total area of the bed joints above and below the test brick. The term v_t, is the value that is exceeded by 80% of all test values, v_{to}. The 0.1 factor in Eq. 1.1 includes corrections for the presence of a collar joint (a vertical mortar joint behind the brick), the relation between peak and average shear stress for a rectangular section (ie., 1.5), an understrength factor of 0.75, and an overall factor of safety of 3.75.

ASTM has recently proposed a standard entitled *In Situ Measurement of Masonry Bedjoint Shear Strength*. This standard covers methods for the determination of the average bed joint shear strength in existing unreinforced solid-unit and ungrouted hollow-unit masonry built with clay or concrete units. Two methods are provided : Method 1 is for determining bed joint shear strength when the amount of vertical compressive stress is controlled with thin hydraulic flat jacks that are placed in the bed joints above and below the test brick. Method 2 is simpler and gives a single value of shear strength based on the insitu vertical compressive stress. RILEM has also proposed a similar method recently.

Pioneering research on the in-place shear test was done by Kariotis et el. (Ref. 1) with the ABK research program. This test was adopted by the City of Los Angeles for their URM evaluation standard, and was later used to formulate the UCBC provisions. Noland et. el. (Ref. 15) modified the in-place shear test to include a way to vary the vertical compressive stress with flat jacks which was the basis of the ASTM Method 1 mentioned above.

1.4 Outline of Report

The experimental work is described in Chapter 2. Results of the experiments are presented in Chapter 3. Implications of test results are discussed in Chapter 4. Summary and conclusions are in Chapter 5.

CHAPTER 2.
EXPERIMENTAL WORK

The outline of experimental work is presented in this chapter. The basic loading system is first described which is followed by a description of the masonry wall specimens, the instrumentation, and the masonry materials.

Three unreinforced masonry walls were tested in the Newmark Civil Engineering Laboratory. The walls were subjected to in-plane shear forces according to a predefined cyclic loading pattern. Before ultimate load testing of the walls, non-destructive tests were performed to evaluate lateral force capacity. Two variables were considered for the experiments : wall aspect ratio, and vertical compressive stress.

2.1 Loading System

A typical wall in the loading rig is shown in Figs. 2.1 and 2.2. The boundary conditions at the top and bottom of a wall test specimen emulated a cantilevered element, with both vertical and horizontal loading applied at the top of the wall. Horizontal forces were applied at the center-
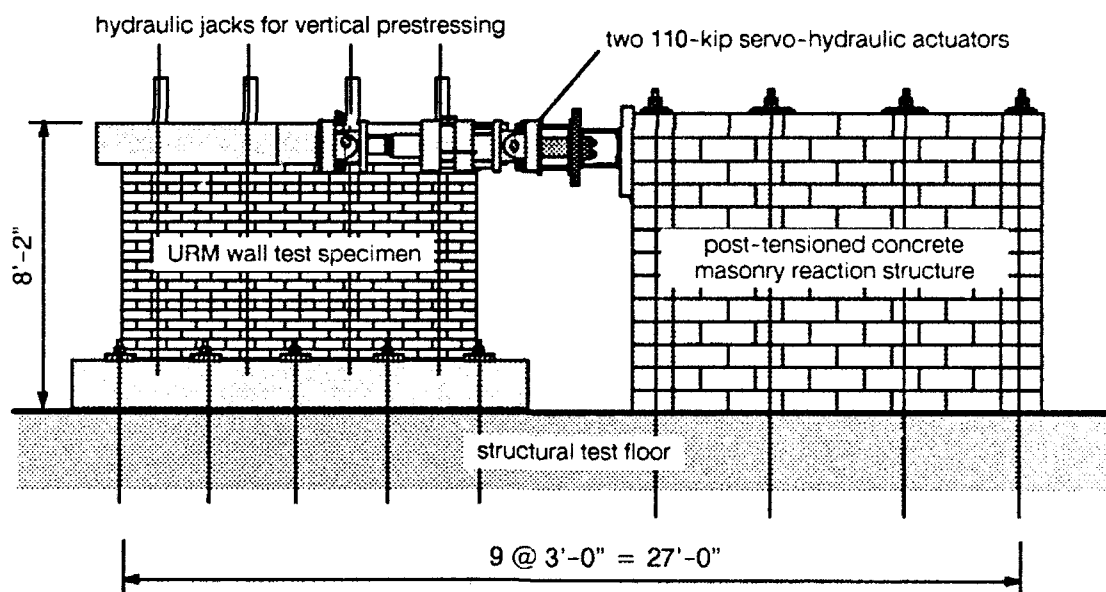

Figure 2.1   Loading Rig and Wall Test Specimen

line of a test wall using a twin pair of 110-kip capacity servohydraulic actuators that were reacted against a stiff post-tensioned concrete masonry reaction structure. Details on construction and utilization of the reaction structure can be found in Ref. 18. Vertical compressive forces were applied at the top of a wall specimen with a series of four pairs of hydraulic jacks. The jacks were reacted with steel prestressing bars that were anchored into a concrete foundation pad. Vertical forces were applied on the top of a concrete beam (Fig. 2.3) that distributed the forces to the top of a wall specimen evenly.   The concrete beam was also used to distribute horizontal forces.

Figure 2.2   Test Wall in Rig

The concrete foundation pad was prestressed to the strong floor so that it would not slide. Ten (1.75" diameter) Dywidag steel prestressing bars were used to clamp the pad to the floor. Dabs of hydrocal were placed at the pad–floor interface to verify that the base did not slide during a test. Since no cracking of the hydrocal was observed, it is certain that the base did not slide. The foundation pad was 14'-0" long and had a rectangular section with dimensions of 60" by 18". The beam was reinforced with #7 bars in both longitudinal and transverse directions.
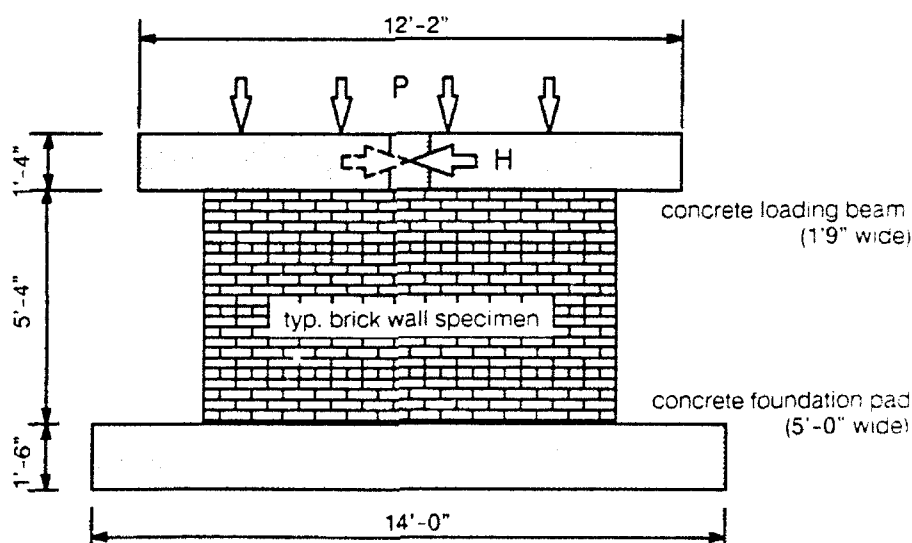

Figure 2.3   Loading Beam and Foundation Pad

Vertical forces were applied using eight hydraulic jacks which were grouped in pairs and positioned at three feet intervals along the length and width of the top beam. Each jack had a capacity of 30 tons, and was pressured with a hand pump. A total of two hand pumps were used, connecting four hydraulic jacks each with a common reservoir so that forces would be equal in all jacks. High strength steel rods anchored in the concrete foundation pad were used to react the hydraulic jacks. A load cell was positioned at each hydraulic jack. Vertical stresses (the total vertical force divided by the gross area of a wall) were 75 psi for specimen W1, and 50 psi for specimens W2 and W3.

The horizontal load was applied to the flanges of the top concrete beam, which in turn, distributed the lateral forces to the masonry test walls. The first ram was controlled by a predefined sequence of displacements, while the other ram was controlled in accordance with the measured forces in the first ram. In this way, equal forces were applied on both sides of a wall specimen, and control in the post-peak region could be obtained.

2.2 Description of Test Specimens

Each of the three test specimens had a different height-to-length aspect ratio. Since the

(a) Wall Specimen W1

(b) Wall Specimen W2   (c) Wall Specimen W3
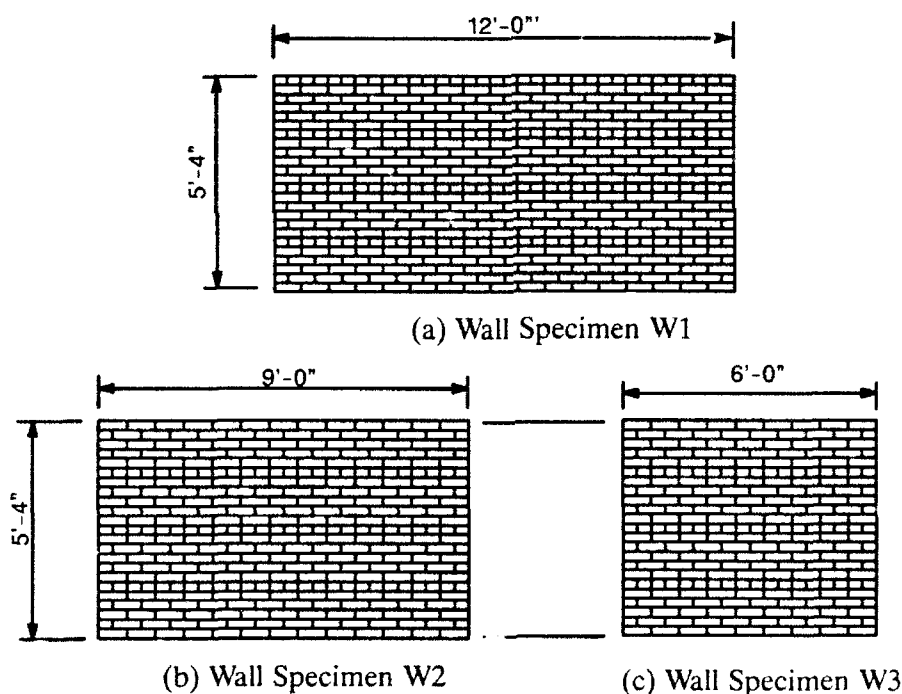
Figure 2.4 Description of Wall Specimens

height was kept the same so that the loading system did not have to be altered, the length of each test wall was varied from 12'-0" to 9'-0" to 6'-0" to give aspect ratios of 2.0, 1.5 and 1.0 for test walls W1, W2 and W3 as shown in Fig. 2.4. A summary of specimen properties is given in Table 2.1.

An American bond pattern was used for each specimen. Bricks were laid in running bond with a header course at every sixth course. Professional bricklayers constructed the walls. Bricks

7

Table 2.1 Specimen Properties

Specimen	L feet	L/h	A_g inches^2	S_g inches^3	I_g x 10^3 inches^4	age days	f_a psi
W1	12.0	2.0	1123	26,960	1,941	120	75
W2	9.0	1.5	842	15,160	819	80	50
W3	6.0	1.0	562	6,740	243	95	50

all specimens: t = 7.8"   n = 6.0 feet

were nominally 7.8" long by 3.5" wide by 2.2" high and were solid with no frogs. The nominal mortar joint thickness was $^3/_8$ inch. The walls were two wythes wide with a collar joint between them. The wall thickness was the length of a brick, or 7.8 inches. The collar joints were filled with slushing of mortar in the cavity. Test wall W1 contained 24 courses of brick while test walls W2 and W3 contained 23 courses each. Because the reclaimed bricks had a high initial rate of absorption, they were soaked in water before placement.

Each masonry wall was set on the base beam in a layer of mortar. The top beam was then positioned on top of each wall, with a layer of mortar between concrete and masonry. The mortar joints were used to transfer the load from the top beam through the masonry wall to the base beam. The mortar mix for these mortar joints was richer then the mortar mix of the walls so that cracks would occur within the specimen and not at the interface with the apparatus.

Wall W1 was tested at 120 days, wall W2 was tested at 80 days and wall W3 was tested at 95 days.

2.3 Instrumentation

During the ultimate load tests, lateral deflection of the test walls was measured relative to their base. In addition, several displacement transducers were mounted on the wall surface to detect local shear and flexural strains. A typical arrangement of transducers is shown in Fig. 2.5. Three vertical transducers were placed along each end of a wall specimen to detect strains resulting from flexure. Two sets of diagonal transducers measured global shear distortions of a test wall.

Distribution of shear along the wall base was determined by the series of transducers across the base. Shear strain for each of the five x patterns of transducers was determined using the following geometrical relation

$$\gamma = \frac{(\delta d_1 + \delta d_2 - \delta v_1 \sin\theta + \delta v_2 \sin\theta)}{2h \cos\theta} \qquad [2.1]$$

where γ is the calculated shear strain across a specified gage length; δd_1 and δd_2 are the measured deformations along the diagonals (elongation is positive for δd_1 and contraction is positive for
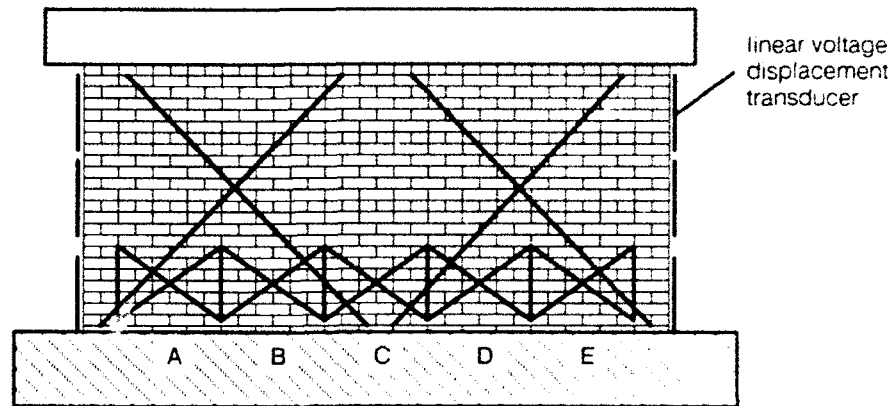
8

Figure 2.5 Arrangement of Displacement Transducers on Wall Surface

δd_2); δv_1 and δv_2 are the measured deformations along the verticals (contraction is positive for δv_1 and δv_2); θ is the angle formed by the diagonals and the horizontal, and h is the height of the wall along which vertical deformations was measured. These variables are shown in Fig. 2.6. The distribution of shear strain can be visualized by plotting the deduced shear strain at each of the five gage points.
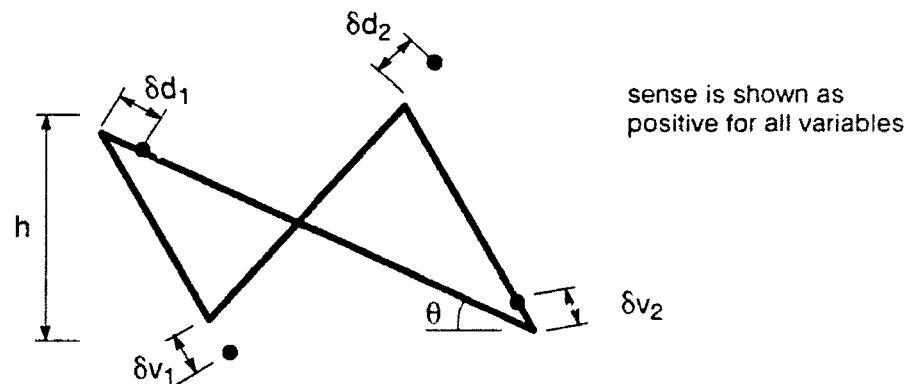
Figure 2.6 Nomenclature for Eq. 2.1

The six vertical transducers along the base of a wall specimen were also used to detect the distribution of vertical strain.

2.4 Masonry Materials

Test walls were intended to represent structures built in the early half of this century. It was important that materials were selected such that test specimens would reflect structural characteristics of an older masonry wall. Based on this criterion, it was decided that solid reclaimed brick with relatively weak mortar be used in construction of test specimens.

Reclaimed bricks were obtained from a distributor in Chicago. Samples from three different lots were chosen and taken back to the Newmark Civil Engineering Laboratory. Several ASTM

9

standard tests were run on the three types of bricks. Among them were the initial rate of absorption, the modulus of rupture and the flat-wise compressive strength. A final selection was made based on the results of these tests. The type of bricks selected had an average compressive strength of 3480 psi with a 6% coefficient of variation. The bricks were of consistent dimension and even shape. A total of seven thousands bricks were then ordered and shipped to Newmark Laboratory for this and another research project.

In order for the test specimens to represent old existing structures, it was necessary to select correct proportions of the mortar mix. To help decide what type of mortar to use, prisms and quadlets (a shear specimen made out of four bricks, Figure 2.7) were built using Portland cement – lime mortar Types N and O, and a lime mortar. Prisms were built with one brick in width and five courses in height. A total of nine prisms were tested using the three types of mortar. These prisms were cured for fourteen days before testing. The prisms were capped at the top and bottom for proper contact with bearing plates and then tested in an universal compression testing machine. The average prism strength was found to be 801 psi for mortar Type N with a 5.5 % c.o.v. The average strength was 565 psi for mortar Type O with 4.8 % c.o.v. and 472 psi for lime mortar with 5.7 % c.o.v. It should be noted that these test results are at 14 days. A 6% to 7% increase could be estimated for 28 days strength (Ref. 19).

Quadlets as shown in Figure 2.7 were tested for shear strength. A total of nine quadlets were
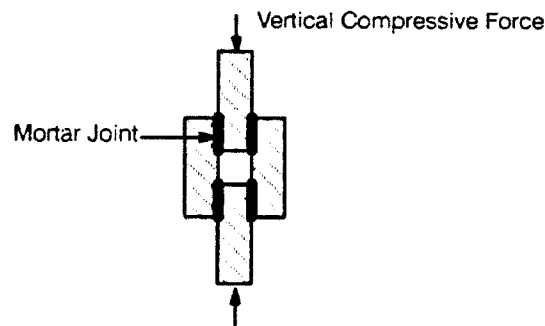

Figure 2.7 Typical Quadlet Test Specimen

built with the three types of mortar. Because of it's zero tensile strength, quadlets made out of lime mortar broke apart upon lifting. The average shear strength was found to be 56 psi for Type N mortar with 49% c.o.v. and 83 psi for Type O mortar with 45% c.o.v. Because of the high data scatter, results of quadlet tests were not given much consideration.

Based on results of the above tests, a decision was made to use Type N mortar for a target prism strength of 1000 psi. This was thought consistent with the strength of brick masonry in the first half of this century (Ref. 16). A total of seven prisms were built at the same time of construction as the wall specimens. After 28 days of curing, these prisms were tested in an universal compression testing machine. The average prism strength was foun : to be 911 psi with a 18% c.o.v.

2.5 In–Place Shear Tests

The in–place shear test is a nondestructive test procedure which measures the strength along the brick–mortar interface of a single brick. A brick unit is pushed in the horizontal direction within the plane of a wall until a sliding movement is sensed (Fig. 2.8). The shear strength is then esti-
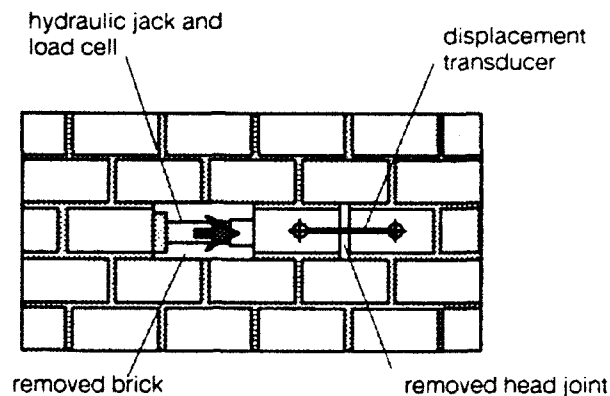

Figure 2.8   Schematic Description of Shove Test

mated as the peak shove force divided by the area of the resisting mortar joints with the amount of gravity stress at the location of test brick being subtracted.

Once a location has been established, a single brick, adjacent to the test brick, is removed by drilling out the surrounding mortar joints. The head joint on the opposite side of the test brick is also removed by drilling out mortar. A displacement transducer is mounted between the center of the test brick and the center of the brick opposite the head joint which is removed to measure sliding of the test brick. The horizontal force is applied to the test brick with a hydraulic jack. The magnitude of the load is measured with a load cell. A typical force–deflection curve for a test brick is shown in Figure 2.9.

By measuring the shear strengths at multiple vertical compressive stress levels, a relationship between the ultimate sliding shear strength and the level of vertical compressive stress was established. This relationship can be represented by the following Mohr–Coulomb relation

$$\tau \; = \; c \; + \; \sigma_v \tan \theta \qquad\qquad\qquad [2.2]$$

where τ = shear strength; c = cohesion coefficient; σ_v = vertical compressive stress; θ = friction angle. Since the vertical stress, σ_v, could be controlled using the test apparatus, various combinations of normal stress and shear strength could be identified. Results of nine of these tests are summarized in Fig. 2.10 where measured shear stress is plotted versus the known vertical stress. Analysis of the test data reveals an average value of cohesion equal to 100 psi and a coefficient of friction equal to 0.50.
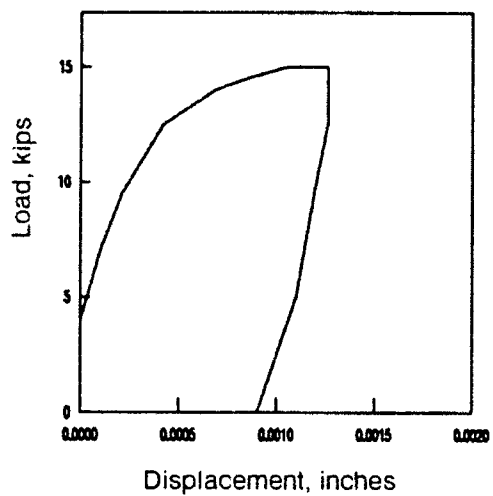
11

Figure 2.9 Typical Shear Force-Deflection
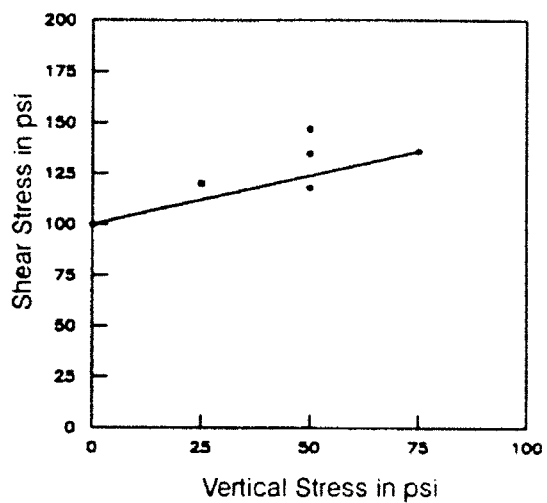Curve for Shove Test

Figure 2.10 Relation between Shear and
Vertical Compressive Stress

CHAPTER 3.
EXPERIMENTAL RESULTS

Results of the ultimate load tests are presented in this chapter for the three wall specimens. Experimental information is given on crack patterns and damage, and their relation to observed lateral strength and stiffness characteristics.

3.1 Cracking and Damage of Wall Specimens

The first wall, W1, failed in shear with no flexural cracking. This was expected since the wall was stocky with an aspect ratio of 2.0. At a lateral force equal to approximately 62% of the ultimate load, a stair-step diagonal crack (marked with the letter a in Figure 3.1a) was observed. A second diagonal crack (marked with the letter b) was observed just as the test wall was reaching its peak lateral strength. The ultimate limit state for specimen W1 was diagonal shear cracking. It should be noted that the limit state was reached after the second diagonal crack formed. This suggests that a considerable redistribution of shear stresses had occurred after formation of the first crack, and refutes the generally accepted opinion that behavior of unreinforced walls in shear is always a brittle phenomenon.

westward loading   eastward loading

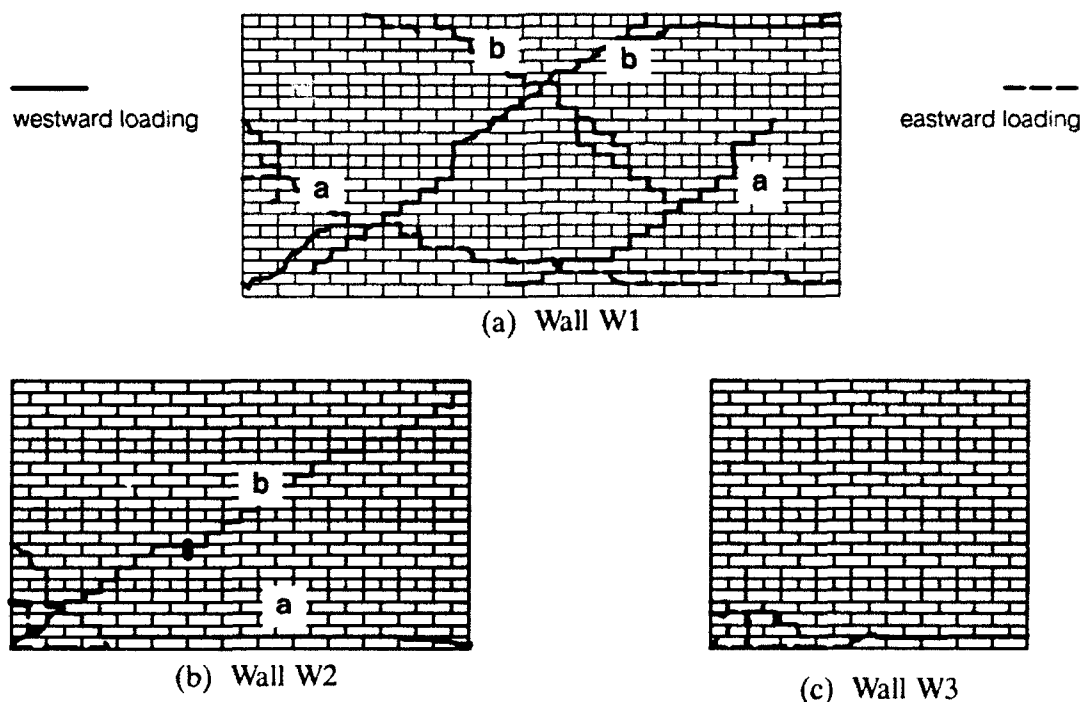(a) Wall W1

(b) Wall W2

(c) Wall W3

Figure 3.1   Observed Cracked Patterns

The second wall, W2, being less stocky than the first, and subjected to a lighter vertical compressive stress, cracked initially in flexure. A horizontal crack along the bed joint immediately above the bottom course was observed along approximately two-thirds of the base (marked with

the letter *a* in the Figure 3.1b). Only until the very last half cycle of loading did a diagonal shear crack occur (marked with letter *b*). This diagonal crack did not occur at the peak loads of the earlier cycles, but after the same maximum lateral force had been reached several times.

The shear crack for specimen W2 was a result of a lateral deflection rather than the lateral force. It is surmised that with increased lateral deflection, the flexural crack grew in length, and shear stress continued to be redistributed to the ever shrinking compression zone near the toe of the wall. Thus, the concentration of shear stress increased though the lateral force did not, until diagonal cracking occurred. Because the vertical force was held constant during the test, the total restraining frictional force along the base of the wall remained constant though the resultant vertical force had to shift across the wall to near the toe. This implies that flexural cracking did not tend to reduce the overall shear strength which is the reason why the diagonal tension strength could be reached well after flexural cracks were first observed.

Vertical splitting cracks, and spalling of bricks was observed at the toe of specimen W2 (Fig. 3.2) much like that for a masonry prism subjected to concentric vertical compression. This condition represented the ultimate limit state of the wall. A toe compression failure such as this may be construed to be a flexural failure, however, it was precipitated by diagonal shear cracking. Thus, the limit state for specimen W2 may be classified as a flexure–shear failure.

Figure 3.2 Toe Crushing for Specimen W2

The third test wall, W3 being a slender one, cracked entirely in flexure. A horizontal crack along the bed joint immediately above the bottom course was observed along approximately 80% of the length of the base (Fig. 3.1c). When the lateral force was reversed, the flexural crack occurred on the opposite side of the wall and was then continuous along the entire length of the wall. The ultimate limit state for specimen W3 was clearly a flexural failure that was initiated by flexural tensile cracking at the heel, but was reached when the masonry at the wall toe crushed in compression.

3.2 Measured Strength and Behavior

Measured force–deflection relations for the all three walls are presented in Fig. 3.3. Lateral forces were considered positive when in a westward direction or when the actuators were in compression. Displacement transducers were set equal to positive values for westerly lateral movements, or when their core was displaced into the instrument. Thus, the slopes of the force–deflection curves are always positive.

Peak lateral forces, H_{ult}, defining the strength of each wall specimen are summarized in Table 3.1. These values are divided by the wall gross area to give a nominal ultimate shear stress, f_{vu}, which is also listed in the table. Strength in terms of shear stress was largest for the stocky specimen at 85 psi and smallest for the slender specimen at 36 psi. This tendency was attributable to the extent of flexural cracking, and the reduction in available shear area of the uncracked portion as discussed in the next chapter.

Table 3.1 Measured Strengths

| Specimen	L/h	f_a psi	$H_{cracked}$ kips	f_{tu} psi	$H_{ult.}$ + kips	- kips	$f_{vu} = \dfrac{H_{ult}}{A_s}$ psi
W1	2.0	75	-	-	92	98	85
W2	1.5	50	35	115	43	45	52
W3	1.0	50	15	113	20	20	36

The peak strength for all three walls was as high as 1.3 times their initial cracking strength. The striking feature, however, is the fact that the walls could resist lateral force while deflecting to extremely large deflections (2% lateral drift or more). This ductile behavior had to be attributable to friction acting along the bed joints due to the constant vertical compressive stress applied to each test specimen. At very large drifts, mortar head joints were observed to be open to nearly one inch. Thus, the vertical compressive stress made a significant difference on the apparent ductility of the element.

Specimens W1 and W2 were subjected to four loading cycles while Wall 3 was subjected to ten loading cycles. The behavior for loading in one direction did not appear to be influenced by previous damage in the other loading direction. Cracks simply closed as the lateral force was reversed, and the masonry acted as if it were uncracked. Measured force–deflection relations reveal a symmetrical pattern for reversed loading cycles. This corroborates the finding that cyclic behavior for a limited number of cycles may be uncoupled into monotonically increasing load components.
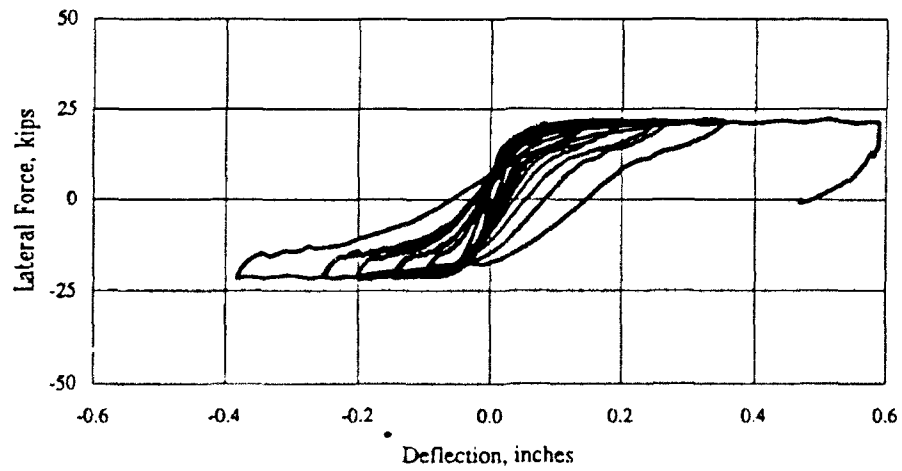
It should be noted from the hysteresis loops for the load–deflection for all three walls that unlike a reinforced member, no change in stiffness (pinching) was observed upon reversal of the load. This is due to the fact that previously opened cracks closed soon after the deflection was
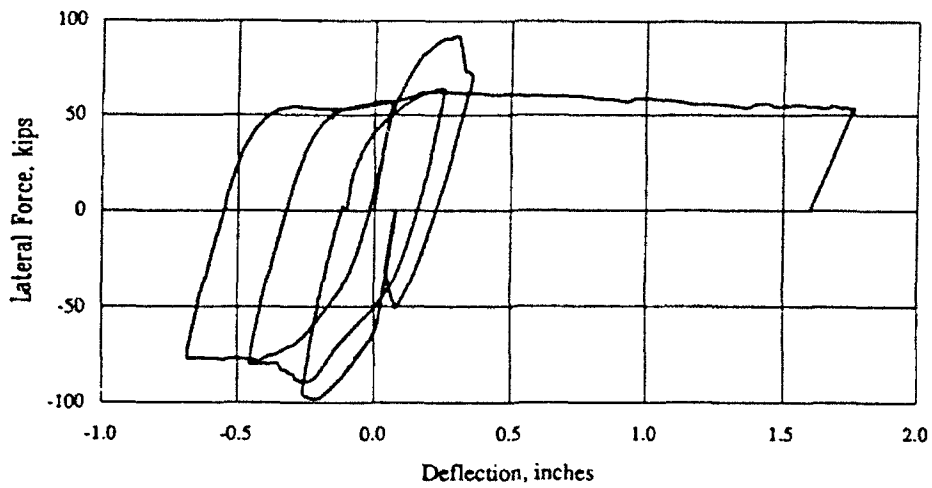
(a) Test Wall W1
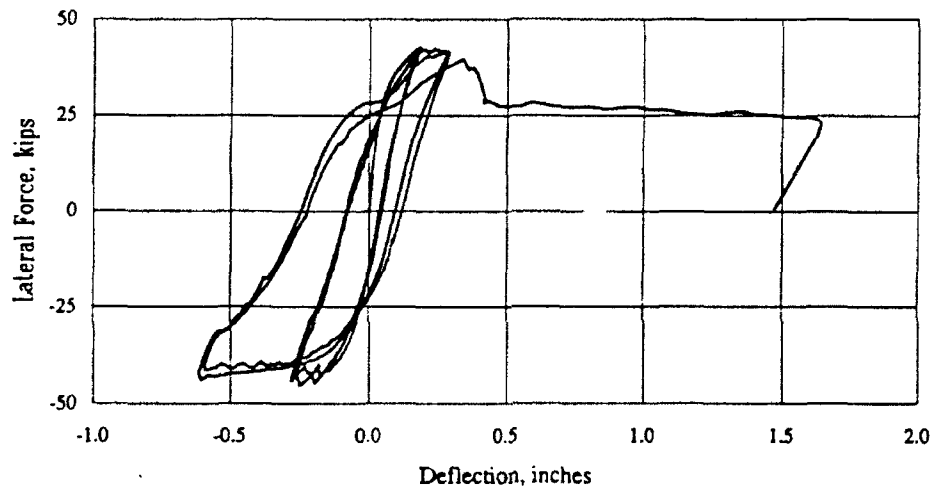
(b) Test Wall W2

(c) Test Wall W3

Figure 3.3 Measured Relations between Lateral Force and Deflection

16

reversed as a result of the vertical compressive stress. Therefore, dissipation of energy through hysteretic cycling, which is proportional to the area contained within the force-deflection loop, would be quite high. This is contrary to the generally accepted notion that unreinforced masonry is a poor dissipater of energy.

3.3 Toe and Heel Deformation

Bending moments result in vertical deformations at the heel and toe regions of a wall that many times limit the lateral strength either through tensile cracking or compressive crushing. Behavior of the test walls is therefore expressed in terms of the measured relations between lateral force and toe/heel deformation in Figs. 3.4 and 3.5. For the purpose of reporting, the *toe* region is that area which sensed compressive stress for positive loading (lateral forces to the west), and the *heel* region is that area which sensed tensile stress for positive loading. Thus, for positive loads, the *toe* region senses compressive stress which is shown as positive in the upper half of the hysteresis curves of Fig. 3.4. When the loading was reversed to a negative sense (in easterly direction), the same region is still termed the *toe* for presentation in Fig. 3.4 although in reality it acts as the *heel*. Deformations become tensile which are shown as negative on the lower half of the figure. *Heel* deformations are generally tensile for positive loadings in the upper half of Fig. 3.5, and are thus negative. Thus, the slope of the curves is generally negative. When the load reverses to a negative sense, the region senses compression and acts as the *toe*, but is still termed the *heel* for presentation in Fig. 3.5. Since the test walls and the loadings are symmetrical, the curves of Fig. 3.4 are similar to those of Fig. 3.5 if they are flipped about their horizontal axes.

Peak vertical compressive strain for all three walls ranged from 0.003 to 0.005. These values are to be expected for crushing of masonry. During unloading, a linear relation between force and deformation was observed suggesting an elastic behavior. Cracks that had opened during loading began to close immediately after the load started to be relieved. This is surmised to be a result of the vertical compressive stress.

3.4 Apparent Flexural Tensile Stress at Heel

Specimens W2 and W3 each cracked in flexure. The lateral force required to crack the heel region, $H_{cracked}$ in Table 3.1, can be inferred from the first change in slope of the plots of Figs. 3.4 and 3.5. These values can then be used to infer the apparent flexural tensile strength using the following common formula for summation of axial and flexural stresses.
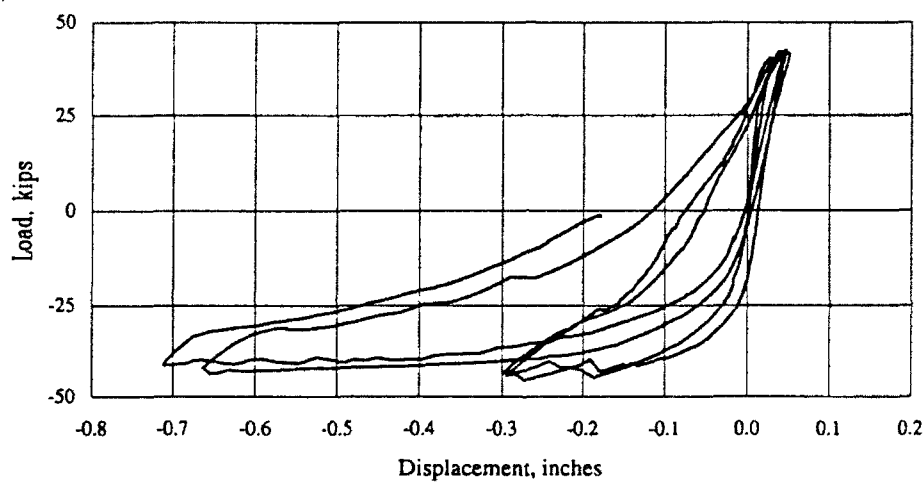
$$f_{tu} = -\frac{P}{A} + \frac{Mc}{I} \qquad [3.1]$$

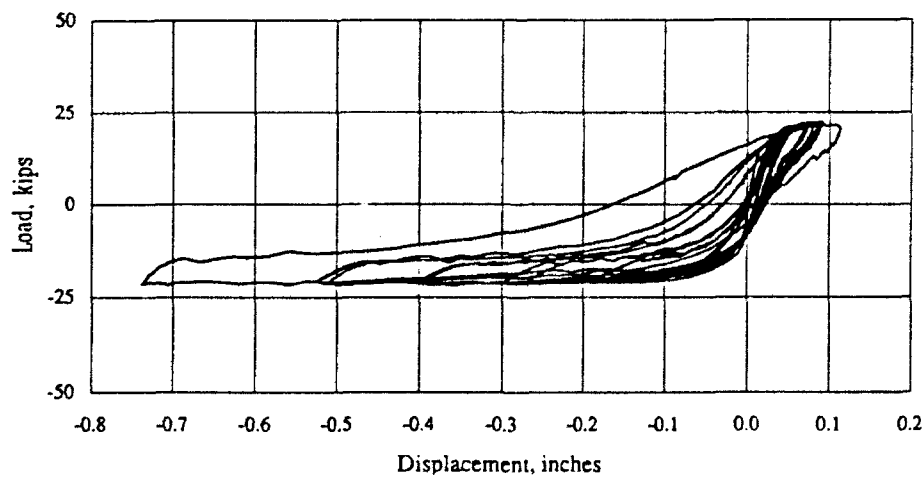$$\text{or} \quad f_{tu} = -\frac{P}{bL} + \frac{6H_{cracked}h}{bL^2} \qquad [3.2]$$

Using measured dimensions of the test walls, the apparent tensile strength of the masonry was found to be equal to 115 psi for W2 and 113 psi for W2 as noted in Table 3.1.
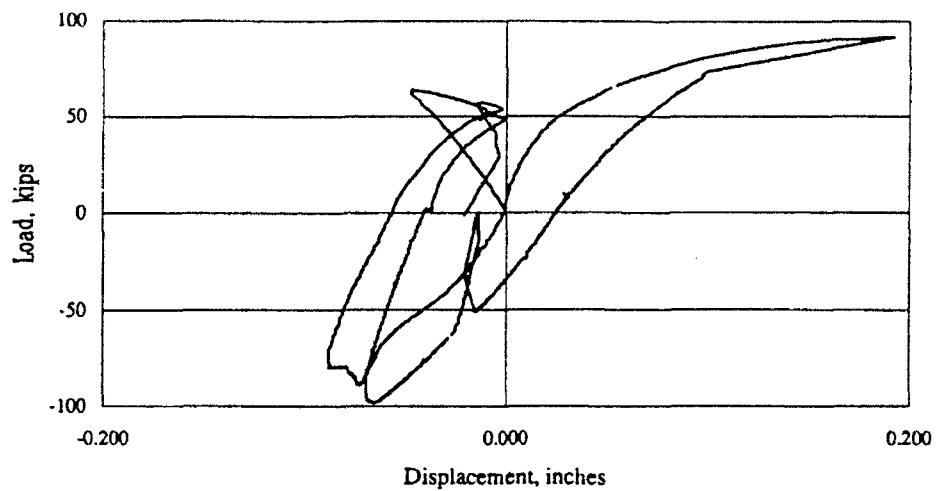
17
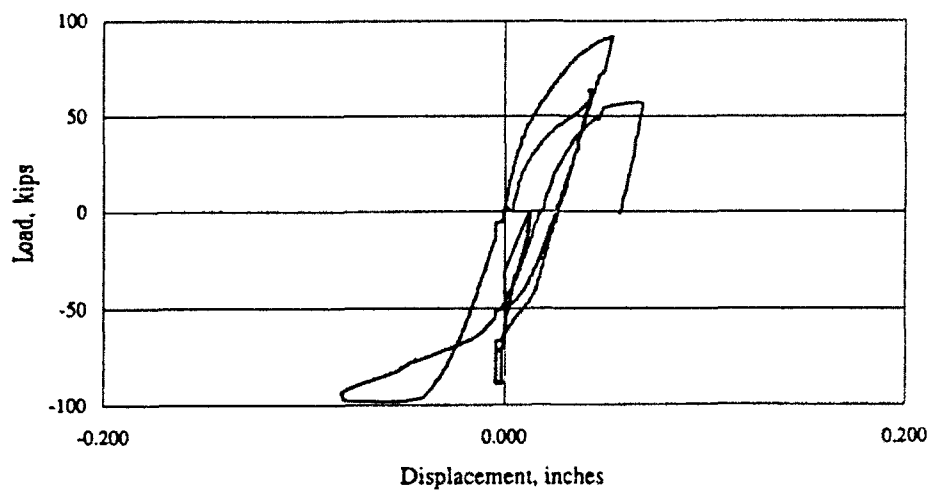
(a) Test Wall W1
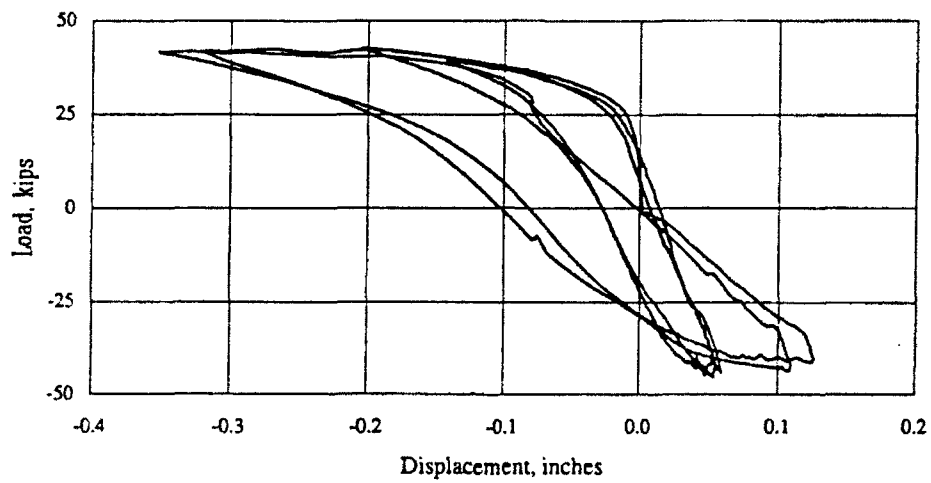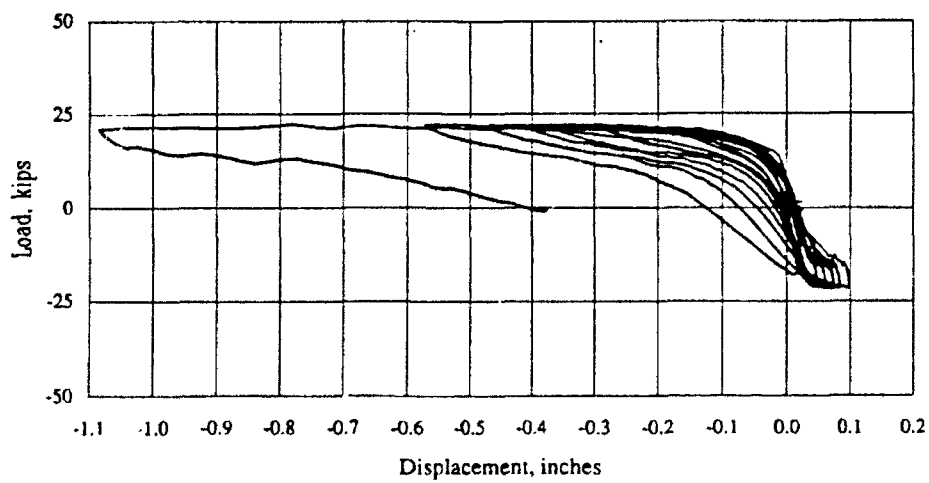

(b) Test Wall W2

(c) Test Wall W3

Figure 3.4 Measured Relations between Lateral Force and Toe Deformation

(a) Test Wall W1

(b) Test Wall W2

(c) Test Wall W3

Figure 3.5 Measured Relation between Lateral Force and Heel Deformation

CHAPTER 4.
INTERPRETATIONS OF OBSERVED BEHAVIOR

Experimental data on strength and behavior of the wall specimens was presented in Chapter 3. In this chapter, measurements are deduced further to show tendencies between each of the three specimens. Four topics are addressed in this chapter: (a) the relation between lateral strength and stiffness for the three wall specimens, (b) the distribution of shear strains across the base of each wall, (c) the distribution of vertical strain across the base of each wall, and (9) how well nondestructive estimates of masonry shear strength approach actual ultimate strengths.

4.1 Comparison of Wall Behavior for the First Quarter Cycle

4.1.1 Force–Deflection Behavior

Lateral force–deflection behavior of the three wall specimens is compared in Fig. 4.1. So
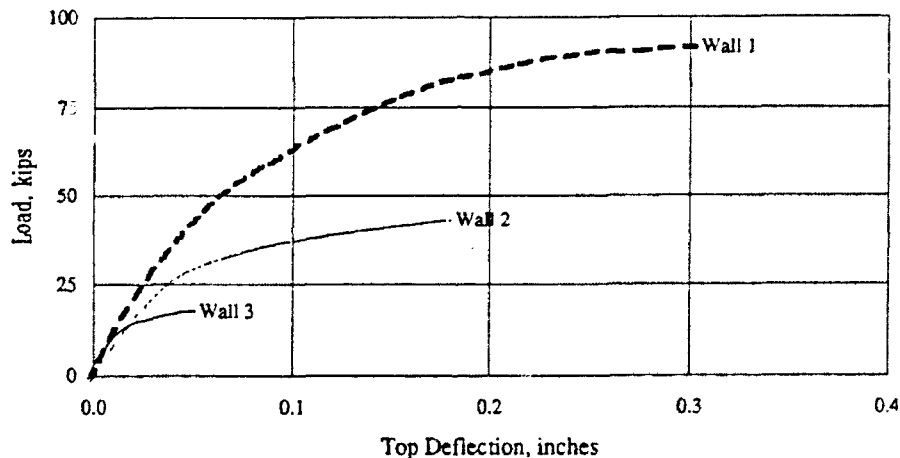

Figure 4.1 Force–Deflection Behavior for the First Quarter Cycle

that direct comparisons can be made between the three curves, measured behavior is shown only for the first quarter cycle of loading. As noted in the previous chapter, wall W1 was governed by shear while walls W2 and W3 were governed by flexure. The gradual softening of wall W1 was attributable to the formation of diagonal cracks (marked with the letter a in Fig. 3.1). The limit on strength for W1 was the formation of the second diagonal crack (marked with the letter b in Fig. 3.1). The sudden changes in slope in the curves for walls W2 and W3 were attributable to flexural cracking at the heel. Peak strength for W2 was limited by diagonal cracking whereas strength for W3 was limited by toe crushing.

It should be noted that peak deflections shown in Fig. 4.1 are those that were arbitrarily set as points of unloading for the first cycle, and do not reflect absolute deformation capacity. However, the lateral deflection at which peak loads occurred are worth noting at 0.30, 0.18 and 0.50 inches for specimens W1, W2 and W3 respectively. In terms of lateral drift (deflection over wall height), these deflections are 0.42%, 0.25% and 0.08%.

Because each wall had a different cross sectional area, it is obvious that the larger wall would be stiffer and stronger than the smaller walls. To obtain a more meaningful comparison, lateral force is divided by the gross area of a wall to give nominal shear stress and is plotted versus lateral drift (deflection divided by the wall height) in Fig. 4.2. It is obvious that the maximum shear stress for each of the three walls was different. The most stocky wall resisted the highest shear while the most slender wall resisted the smallest shear. The initial stiffness, the ratio of shear stress to drift, was similar for each specimen. Both of these aspects are discussed in detail in this section.
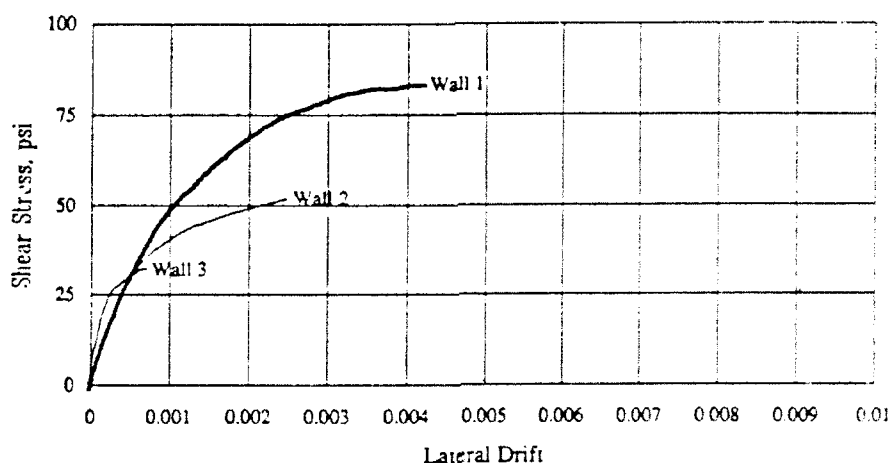

Figure 4.2 Measured Relation between Nominal Shear Stress and Lateral Drift

4.1.2 Lateral Stiffness

It is of interest to note that the initial stiffness was similar for test walls W1 and W2 when expressed as the ratio of nominal shear stress to lateral drift (Fig. 4.2). A common slope of approximately 600 psi per 1% drift was observed for these two specimens. The more slender wall, W3, had a larger normalized stiffness.

A common expression for the lateral deflection of a cantilevered wall is:

$$\delta = \frac{Hh^3}{3E_m I_g} + \frac{Hh}{G_m A_s} \qquad [4.1]$$

where H is the horizontal force, h is the wall height, E_m is the elastic modulus of masonry in compression, I_g is the gross moment of inertia, G_m is the masonry shear modulus, and A_s is the shear area of the wall. The first term in Eq. 4.1 represents the flexural deformations while the second term represents the shear deformations. The equation is based on elastic theory for an uncracked wall, and its derivation can be found in most textbooks on structural analysis.

Substituting $L^3 t/12$ for I_g, noting that the shear area is equal to 5/6 the gross area, Lt (for a rectangular section), assuming that G_m is equal to $0.4 E_m$, and dividing by h in Eq. 4.1 gives:

22

$$\frac{\delta}{h} = \frac{4Hh^2}{E_mL^3t} + \frac{1.2H}{0.4E_mLt} \tag{4.2}$$

Noting that the nominal shear stress, f_v, is H/Lt, and factoring reduces Eq. 4.2 to:

$$\frac{\delta}{h} = \frac{f_v}{E_m}\left[4\left(\frac{h}{L}\right)^2 + 3\right] \tag{4.3}$$

from which the following expression for the slope (ratio of stress to drift) can be derived

$$\frac{f_v}{\delta/h} = \frac{E_m}{\left[4(h/L)^2 + 3\right]} \tag{4.4}$$

For the three aspect ratios ($L/h = 2.0$, 1.5 and 1.0), the initial slope of the curves in Fig. 4.2 should be according to Eq. 4.4 equal to 0.250, 0.209 and 0.143 times E_m for wall specimens W1, W2 and W3 respectively. Assuming a value of 750 times f_m for E_m (which was measured at 911 psi) results in calculated values of the slope equal to 171, 143 and 98 psi per % drift for the three test walls. These values are very much less than the measured values of 610, 610 and 1170 psi per % drift (Fig. 4.2) suggesting that the test walls were much stiffer than what the calculations would suggest.

4.1.3 Ultimate strength

Each of the three walls and limit states resulted in a different lateral strength. Wall W1 had the highest strength (nominal shear strength of 85 psi) while walls W2 and W3 had strengths of 52 and 36 psi respectively. Shear strengths increased with aspect ratio as shown in Fig. 4.3. The slightly disproportionately high value for W1 may have been attributable to the larger vertical compressive stress.

The trend in lateral strength is corroborated by a simple theory proposed by Abrams in Ref. 2 that limits strength by toe compressive stress according to the following formula where f_{va} is the allowable average shear stress, f_a is the vertical compressive stress, L/h is the length-to-height aspect ratio, and F_a is the allowable toe compressive stress. The equation is based on the post-cracking behavior of a wall that is cracked in flexure. After initial cracking at the heel of a wall, the vertical force resultant shifts towards the wall toe until vertical stress exceeds the allowable compressive stress.

$$f_{va} = f_a\left(\frac{L}{h}\right)\left[\frac{1}{2} - \frac{2}{3}\frac{f_a}{F_a}\right] \tag{4.5}$$
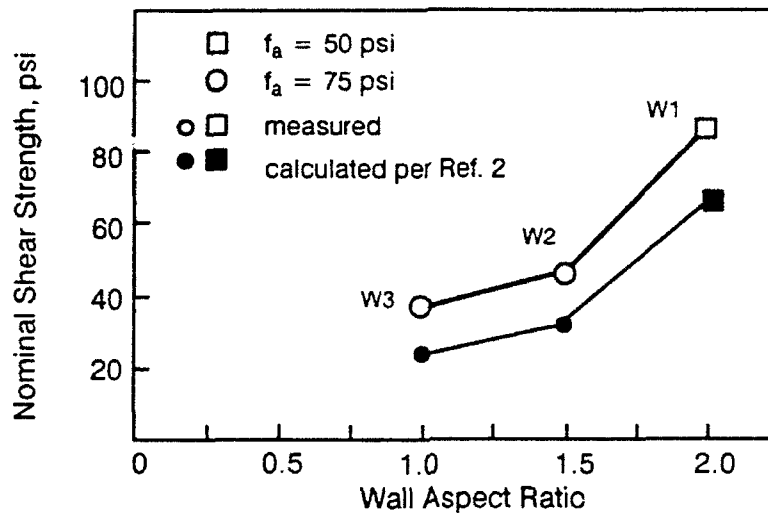
23

Figure 4.3 Observed Relation between Shear Strength and Wall Aspect Ratio

For purposes of comparison with the measured ultimate shear strength, f_{va} is replaced with f_{vu} by substituting f_m for F_a. The measured prism strength is 911 psi as noted in Chapter 2. Strength estimates calculated using Eq. 4.5 are plotted on Fig. 4.3 for comparison with the measured data. Whereas the strength estimates are lower, and thus conservative, they do follow the same tendency with respect to aspect ratio as the measured data. This is somewhat surprising since the formulation for Eq. 4.5 is based on a flexural mechanism, and wall W1 failed in shear.

Lateral force is plotted versus toe deformation for the first quarter cycle of each test wall in Fig. 4.4. The initial value for the toe deformation for specimens W2 and W3 is a result of the
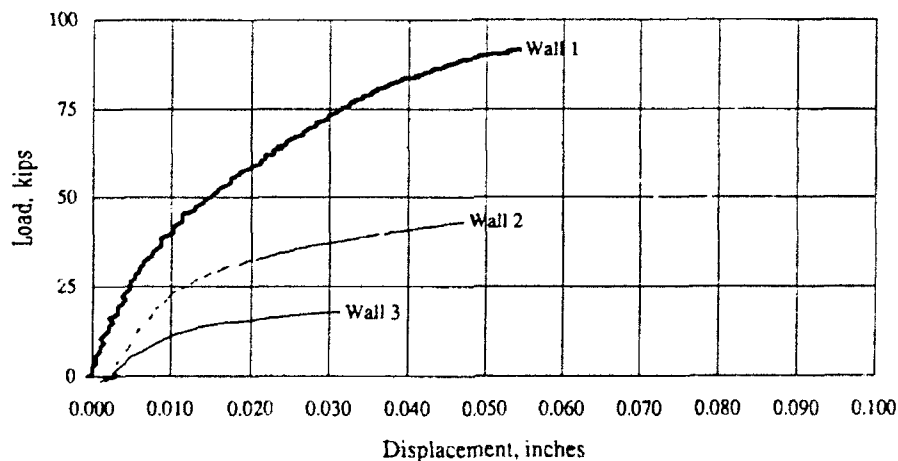

Figure 4.4 Measured Relation between Lateral Force and Toe Deformation

vertical stress that was applied after the zero transducer reading was taken which was not done for specimen W1. The peak compressive strains were on the order of 0.005 for walls W1 and W2 and 0.003 for W3. These values are within the expected range for masonry near crushing, and

correlate with the observed damage. The rather high compressive strain for wall W1 is of interest since the wall failed in shear.

4.2 Distribution of Shear Strain along the Wall Base

As described in Chapter 2, shear strains across five gage lengths were measured across the base of a wall specimen using the configuration of displacement transducers shown in Fig. 4.5 Readings from the two diagonal transducers were combined with readings from the two adjacent vertical transducers to give a single value for average shear strain across the gage length. A sample relation between lateral force and shear strain is shown in Fig. 4.6 to show the nature of the measurement technique. Force-strain curves for all gage points for all specimens are given in Appendix A.
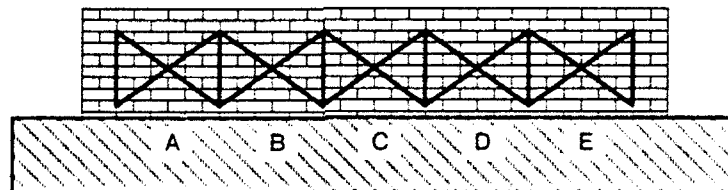
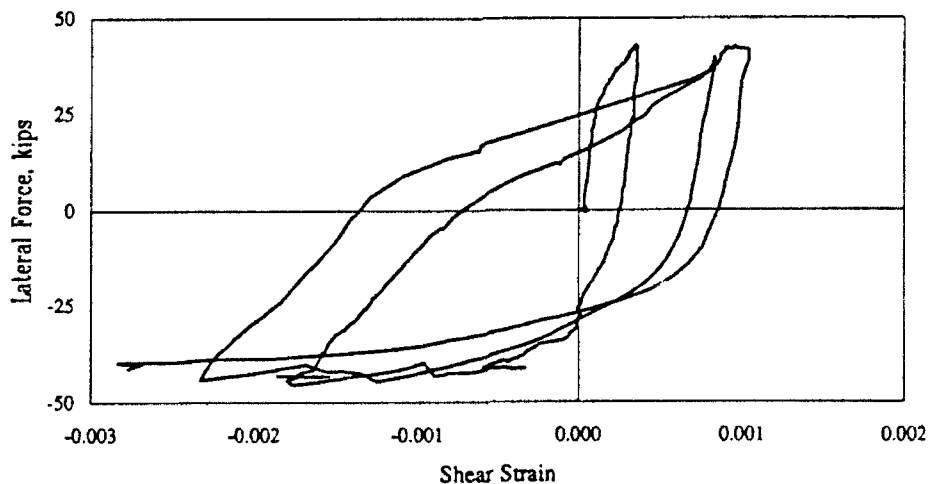
Figure 4.5 Shear Distortion Measurement Locations

Fig. 4.6 Typical Relation between Lateral Force and Shear Strain
(Specimen 2, point A)

Strain measurements for all five gage points are plotted in Figs. 4.7 and 4.8 to show the apparent distribution of shear strain along the wall base. Distributions are shown for a few representative load levels during the first quarter cycle of loading in Fig. 4.7. Shear strain distributions are for loading to the west or to the left in the figure. Thus the toe region is on the left-hand side of the distribution. Curves shown in Fig. 4.8 demonstrate the nature of the distribution at first un-
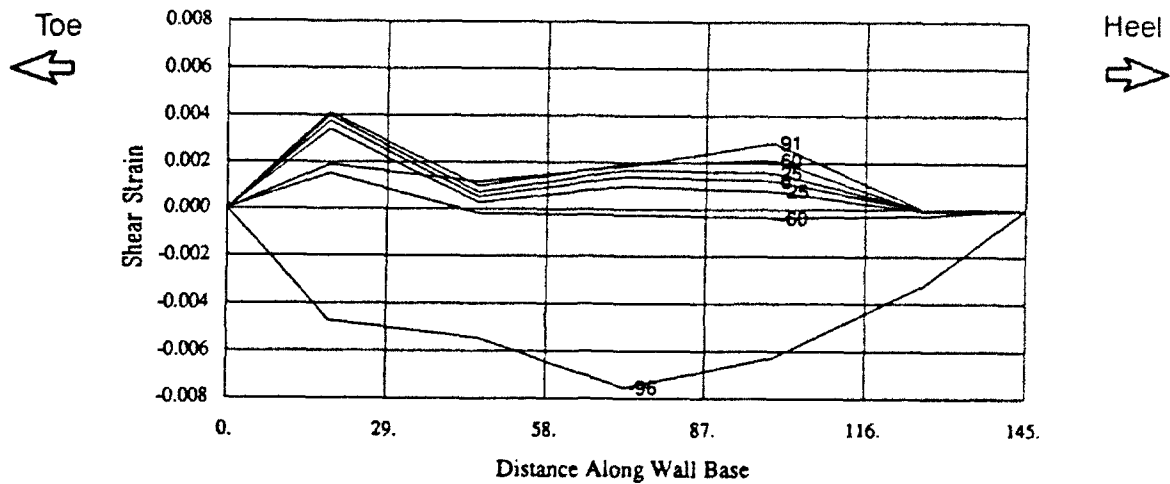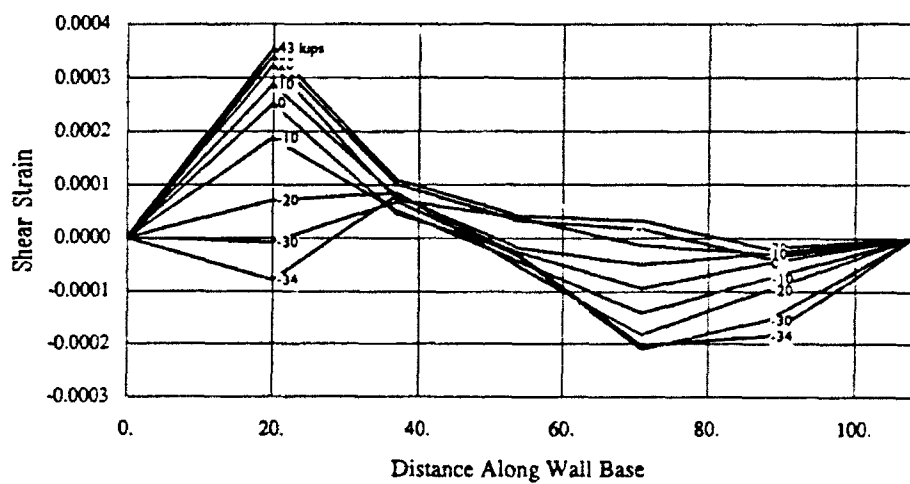
Toe

Heel
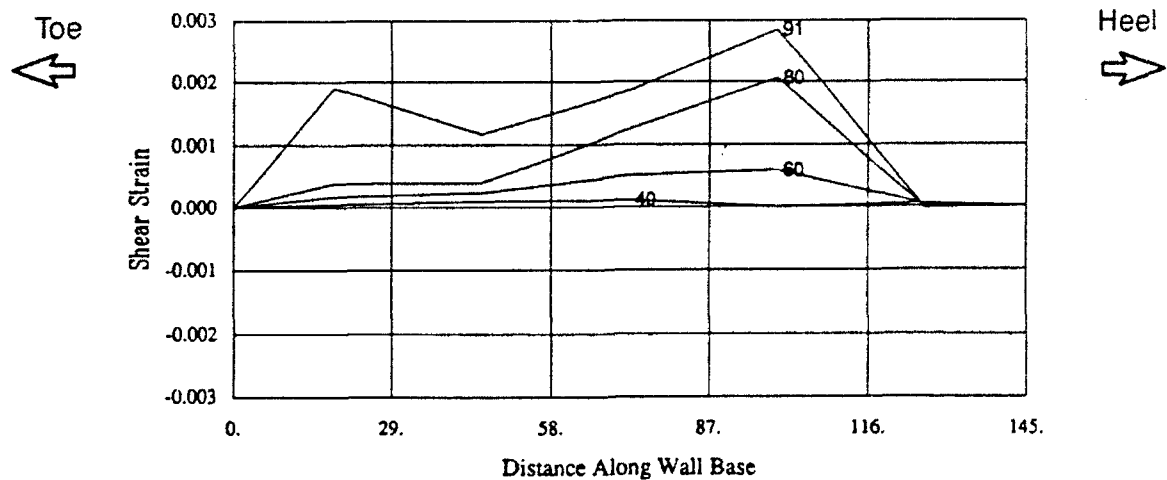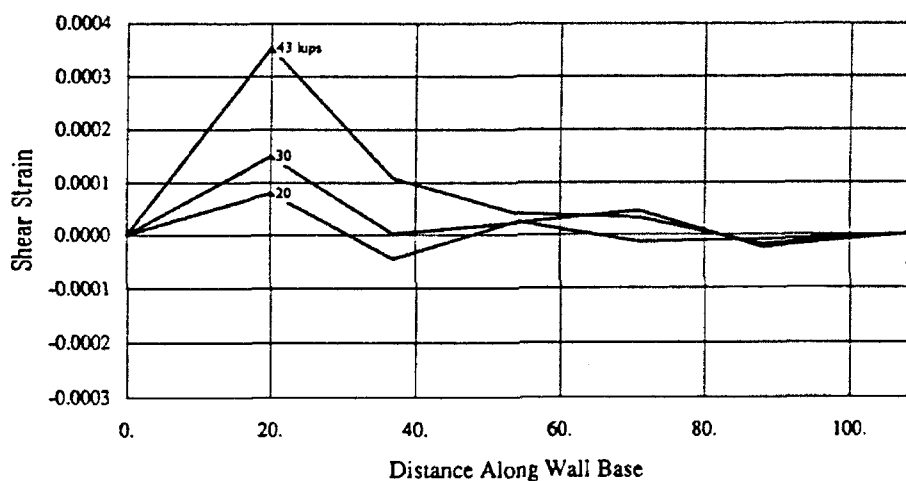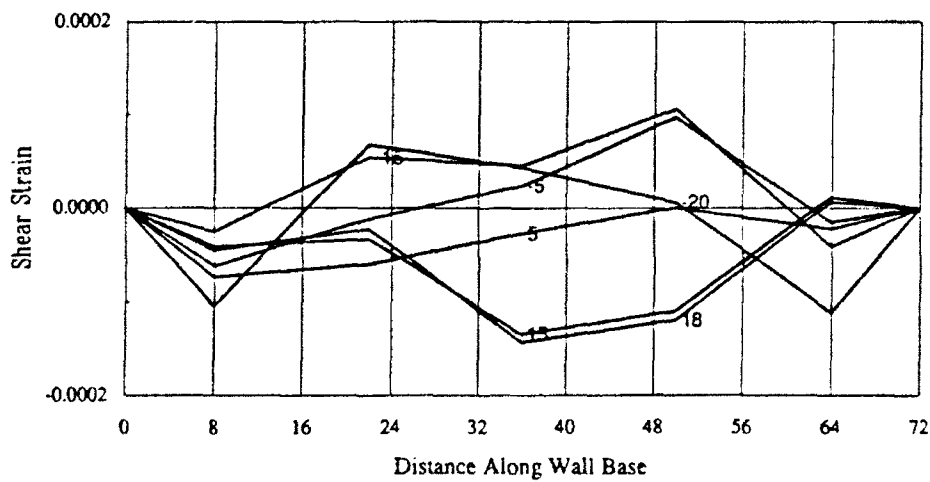

(a) Specimen W1
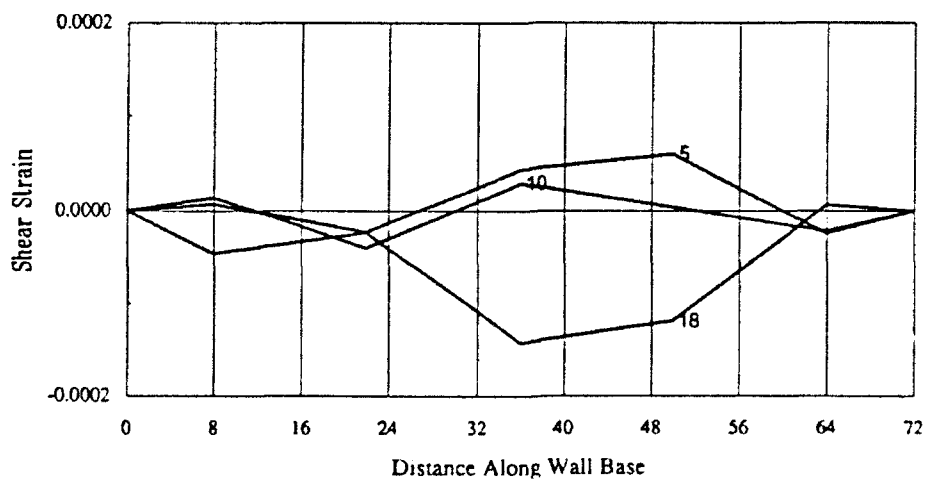
(b) Specimen W2

(c) Specimen W3

Figure 4.7 Distribution of Shear Strain for the First Quarter Cycle

26

Toe ⇐   Heel ⇒

(a) Specimen W1

(b) Specimen W2

(c) Specimen W3
Figure 4.8 Distribution of Shear Strain for the Second and Third Quarter Cycle

loading (the second quarter cycle) and at first reloading (the third quarter cycle) where the lateral force is applied to the east, or to the right in the figure.

Inferring shear strain distributions from the five sets of displacement transducers is a new method that was tried for the first time with this laboratory study. The measurement method is an experiment in itself. It is evident by examining Figs. 4.7 and 4.8 closely that there are some irregularities in the shear strain distributions that may be attributable to effects other than the shear straining of the masonry. One major influence on the accuracy of the measurement is the propagation of cracks through the gage lengths. When this happens, nearly all of the measured deformation is a result of cracks opening and not straining of masonry. In addition, because any-one shear strain computation is based on four independent transducers (and sometimes the difference between transducers) small instrument errors may be amplified. However, a few tendencies do emerge from the distribution plots that suggest possible behavioral modes.

Shear strain distributions for wall W1 approached the parabolic distribution that is expected for a linear, uncracked wall (f_v = VQ/Ib). Because wall W1 did not crack in flexure, shear was being distributed across the entire wall length. When load was reduced, shear strains reduced but maintained the same distribution. When the direction of load was reversed, the distribution followed the same pattern and resembled the common parabolic distribution.

The influence of flexural cracking on shear strain distribution can be seen with wall W2 which cracked in flexure along a bottom bed joint. Only the toe region of the wall sensed shear because no shear stress could be transferred across an open flexural crack. Upon unloading, shear strains in the toe region reduced to zero but kept the same distribution. When lateral force was reversed, the same tendency was observed with the toe region (now, right-hand side) attracting nearly all of the shear.

Shear strain distributions are not meaningful for wall W3 because the amount of shear stress was light. The relatively slender wall cracked in flexure at the base at a small level of shear stress. Shear strains were small, and it is not plausible to infer tendencies regarding distribution effects.

4.3 Vertical Strain Distribution

As noted in Chapter 2, vertical strain was measured at six different points along the wall base with vertical displacement transducers as shown in Fig. 4.9.
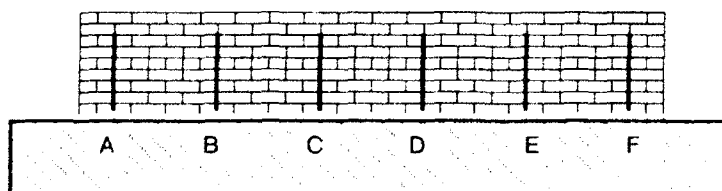

Figure 4.9 Vertical Strain Measurement Locations

Measured relations between lateral force and strain at each point for the three wall specimens are presented in Appendix A for reference. Distributions of vertical strain for a few representative load levels during the first quarter cycle of loading is shown in Fig. 4.10 for the three specimens. Positive strain values are for compression. Loading was to the west, or to the left in the figure. It is clear that each wall specimen was sensing compression at the toe region (on the left hand side) and tension at the heel region, as would be expected. The location of the neutral axis could also be inferred from the distributions.

The vertical strain distribution for wall W1 is somewhat inconclusive because of the relatively light flexural stresses, and because of the anomaly at point D which was a result of crack a (Fig. 3.1) propagating through the gage length. However, at lateral force levels below 50 kips, wall W1 did sense compressive strain on the left and tensile strain on the right. The location of the neutral axis was near the centerline of the wall as would be expected.

Vertical strain distributions for walls W2 and W3 clearly indicate that the neutral axis was shifting towards the toe (to the left in Fig. 4.10) as the lateral force was increased. This finding is in agreement with the observed crack development along the base of each wall. The distribution of vertical compressive strain is nearly linear suggesting that the masonry was behaving as a linear material, and that a simple triangular stress distribution (as commonly assumed) would be admissible. Compressive strain at the toe is seen to increase disproportionately with lateral force as would be expected as the uncracked compression zone continues to shrink. This finding strongly suggests that the ultimate limit state for flexural action is toe crushing and not tensile cracking.
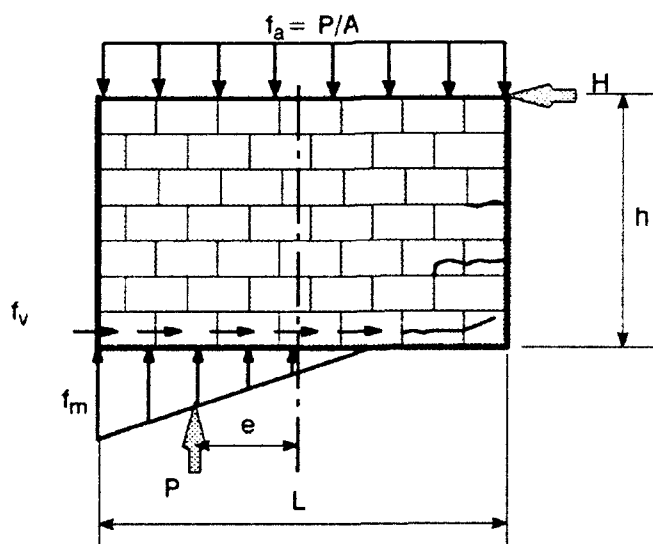

Figure 4.11. Free Body Diagram of Wall Cracked at Base.

As lateral force is increased and the flexural crack across the base of wall, the resultant of the vertical force continues to shift towards the toe until compressive stress is exceeded. Thus, an unreinforced wall with no tensile strength can resist lateral force, H, and overturning moment, Hh, through the vertical force couple that is created when the resultant force, P shifts a distance e from the centroid as depicted in Fig. 4.11.
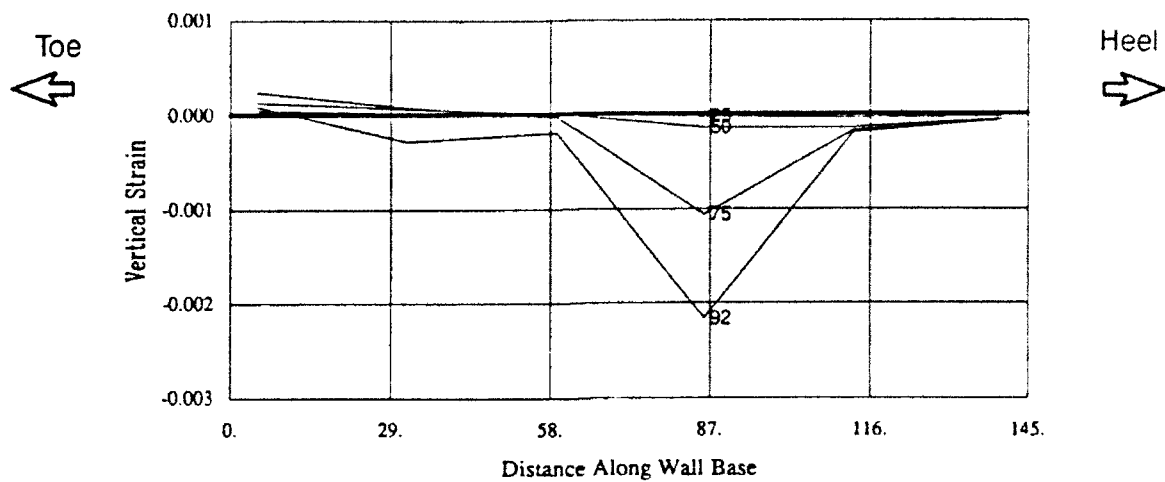
(a) Specimen W1
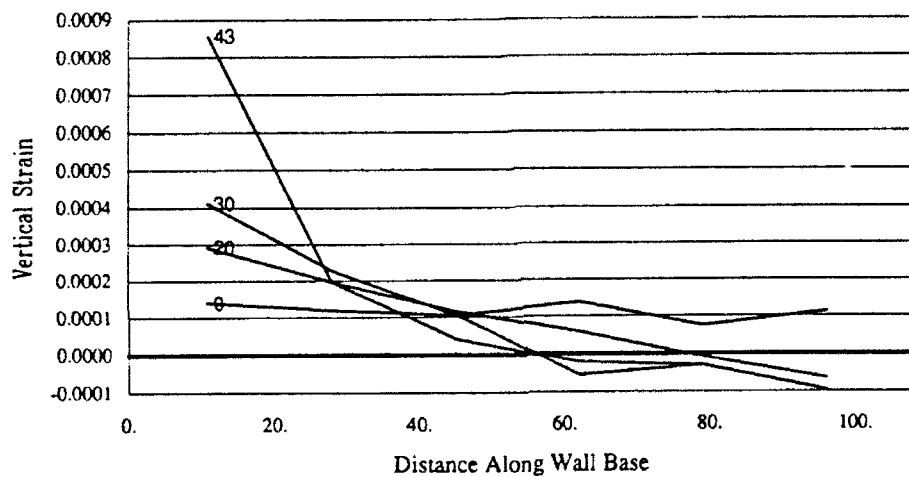
(b) Specimen W2
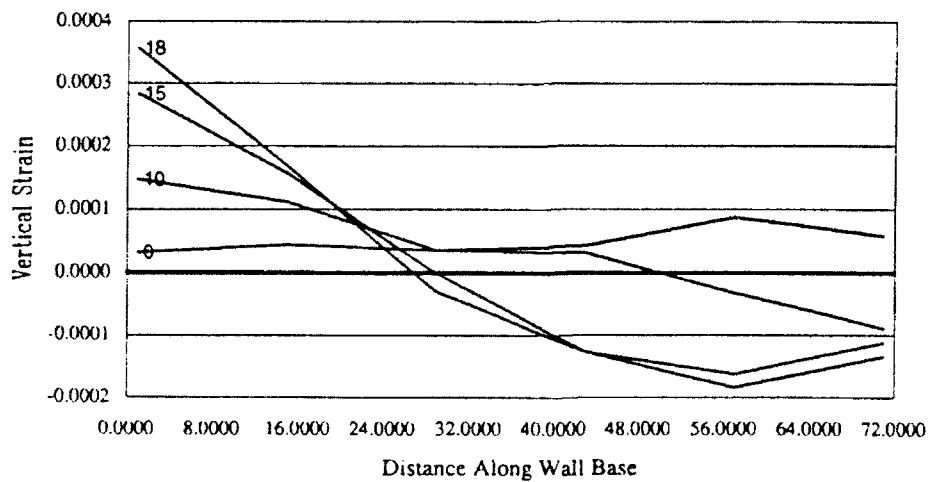
(c) Specimen W3

Figure 4.10 Distribution of Vertical Strain for the First Quarter Cycle

Before the lateral force was introduced, a nearly uniform vertical strain distribution was measured for each of the two walls which was a result of the vertical stress that was applied. The even distribution verifies the fact that the forces applied by the series of vertical jacks were evenly dispersed across the wall length.

4.4 Correlation between Ultimate Shear Strength and NDE Estimates

Since very few actual unreinforced masonry walls have been tested to failure, the evidence needed for verification of nondestructive estimating methods of wall strength is scant. Therefore, the measured ultimate strengths of the three test walls provide useful information on the accuracy of NDE methods. As described in Chapter 2, one such method is known as the "in-place shear test" or "shove test." The test measures masonry shear strength at a single point. The question that is explored with this study is how shear stress at a point can be integrated across the area of a wall to give lateral component strength when a portion of the wall is cracked.

The previous discussion of the influence of flexural cracking on shear strain distribution suggested that shear stress is resisted only within the compression zone. The cracked, tension zone (for walls controlled by flexure) does not resist shear because stress cannot be transferred across an open crack. Thus if a wall is cracked in flexure, it is not correct to rely on the full gross area to resist shear, but rather a portion of the wall area. Correlations are made in this section between the ultimate shear stress resisted by the three test walls and the shear stress that would be predicted by various procedures.

A description of the in-place shear test is given in Chapters 1 and 2. The following formula, which was presented as Eq. 1.1, has been adopted by UCBC (Ref. 20).

$$v_a = 0.1v_t + 0.15\frac{P_D}{A} \qquad [4.6]$$

The term, v_t, is the 20% percentile of in-place shear test data that have been reduced to a zero gravity stress. The 0.1 factor times v_t does not imply a safety factor of 10. A number of reduction factors have been applied to the following equation to obtain Eq. 4.6.

$$v_u = \frac{\frac{3}{4}\left(\frac{3}{4}v_t + \frac{P_D}{A}\right)}{1.5} \qquad [4.7]$$

where v_u is the estimated ultimate shear strength. The denominator of 1.5 is used to translate peak shear stress to average shear stress across a rectangular section. The first 3/4 factor is an understrength factor. The 3/4 factor applied to v_t is a correction factor to account for possible shear resistance provided by a collar joint. An overall safety factor of 3.75 is then applied to ultimate values obtained with Eq. 4.7 to give values for allowable stress in Eq. 4.6.

The measured ultimate shear strength of each test wall is compared with three estimates of wall stress in Table 4.1. Data in the table is also plotted in Figs. 4.12 and 4.13. The first set of

Table 4.1 Measured Ultimate Shear Stress vs. NDE Estimates

Specimen	$\dfrac{L}{h}$	f_a psi	measured strength $f_{vu} = \dfrac{H_{ult}}{A_z}$ psi	A $\dfrac{v'_u}{1.5}$ psi	B $\dfrac{\frac{3}{4}\left(\frac{3}{4}v_t + \frac{P_D}{A}\right)}{1.5}$ psi	C $0.1v_t + 0.15\dfrac{P_D}{A}$ psi
W1	2.0	75	85	91	75	21
W2	1.5	50	52	83	63	18
W3	1.0	50	36	83	63	18

shear estimates (shown in Column A of table) represents the most direct comparison with the test data. The shove test measurements are simply divided by a 1.5 factor to account for the difference between average and maximum shear stress. In this case, average shove test values, v'_u, are used with no corrections for vertical stress since the identical vertical stress was applied during the shove test as was used during the ultimate load test (values of v'_u were read from the line given in Fig. 2.10). Thus, no assumptions of frictional coefficients need to be made. Also, because no safety factors are applied, ultimate shove test values can be compared directly with ultimate wall shear stresses.
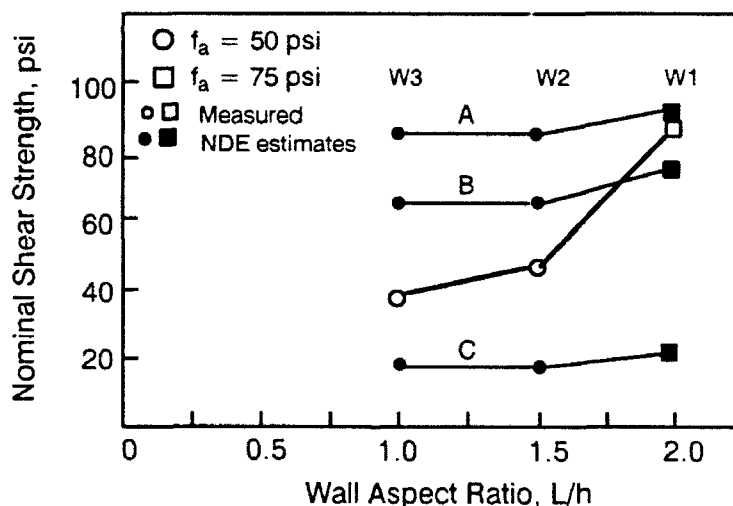

Figure 4.12 Wall Shear Strength vs. Aspect Ratio

Values in Column A are always larger than the measured strengths suggesting that the NDE method is on the unconservative side. For wall specimen W1 which failed in shear with no flexural cracking, the correlation with the measured shear strength (85 vs. 91 psi) is quite close. For the other two wall specimens, W2 and W3, whose behavior was governed by flexural cracking, the actual strength fell far below the estimate (36 vs 83 psi for W3). The deviation between measured and estimated strengths became larger as the L/h aspect ratio reduced. The difference may be

32

attributable to a reduction in the available shear area with flexural cracking as discussed in the previous section. With smaller aspect ratios, the extent of flexural cracking increases and the reduction in shear area reduces.

Results of the second calculation method are shown in Column B of the table. These values have been calculated using a literal interpretation of Eq. 4.7. Values represent a slightly reduced (by the 0.75 understrength factor) but ultimate strength. Data from the in-place shear test have been reduced by a factor of 0.75 to account for a possible presence of a collar joint which was known to exist only partially if at all (the collar joints were slushed with mortar and not filled completely). Also in-place shear test data were reduced to give equivalent values for zero vertical stress for input to Eq. 4.7. Since the measured coefficient of friction was 0.5, and 1.0 is used in Eq. 7, this approach represents friction with larger values than observed.

Because of the various reduction factors used with calculation method B, the NDE estimates approached the measured strengths closer than with calculation method A. Good agreement was seen for wall W1 (75 psi estimated vs. 85 psi measured), however, for wall specimens controlled by flexural cracking, W2 and W3, the estimated values again overshot the measured strengths (63 vs. 36 psi for W3).

Results of the third calculation method are shown in Column C of the table. These values are a literal interpretation of the UCBC formula (Eq. 4.6). Because of the large safety factor (3.75 plus other reduction factors), the estimated values were always less than the measured strengths (as much as 85 vs 21 psi for W1, and as small as 36 vs. 18 psi for W3). The code approach resulted in safe evaluations even though a wall may be cracked in flexure. However, the intention of the large safety factor was not intended to account for these differences. The UCBC formula may need to be reconsidered in terms of shear reductions resulting from flexural cracking.
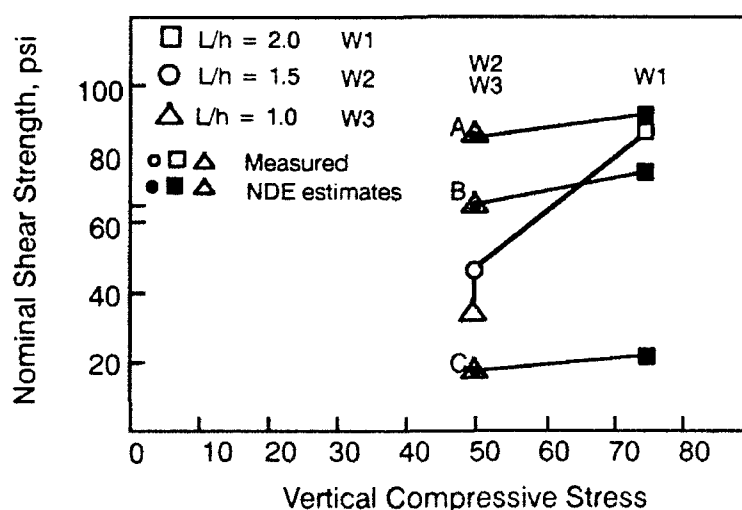

Figure 4.13 Wall Shear Strength vs. Vertical Compressive Stress

By examining Fig. 4.13, it is apparent that there is a larger decrease in shear strength as a result of decreasing vertical compressive stress than the code formulas express. Also, there is a decrease in shear strength attributable to the aspect ratio, L/h, that the code approach neglects. For the same vertical compressive stress (50 psi) specimen W3 had a smaller shear strength than specimen W2. This is again a result of the influence of flexural cracking on shear transfer.

CHAPTER 5.
SUMMARY AND CONCLUSIONS

5.1 Summary of Research

A series of three unreinforced masonry walls were constructed and tested to failure in the Newmark Civil Engineering Laboratory. The test walls were subjected to vertical compressive stress and lateral deflections. The length-to-height aspect ratio, and the vertical compressive stress, was varied for each test wall. The insitu sliding shear strength between brick-mortar interfaces was measured before the ultimate load tests using a nondestructive technique so that correlations between actual strengths and estimates could be made.

5.2 Conclusions

1. Test walls resisted considerable lateral force after the formation of the first crack. For test walls controlled by flexure, the resultant of the vertical compressive stress shifted towards the toe after initial flexural cracks formed, and thus provided a lever arm to react overturning moments. For the test wall controlled by shear, the vertical compressive stress provided sufficient frictional force to resist lateral loads after the formation of stair-stepped diagonal tension cracks.

2. Test walls resisted lateral forces in a ductile manner. Even the specimen failing in diagonal tension could sustain lateral drifts in excess of 2% while resisting forces over 60% of its peak strength.

3. Test walls behaved elastically when lateral force was relieved. Previously opened cracks closed soon upon unloading because of the restoring nature of the vertical compressive stress. Unlike a reinforced member, no sudden changes in stiffness were observed when the direction of load was reversed. Thus, the area contained by a hysteresis loop was large, and energy dissipation would be high for reducing vibrations.

4. Behavior for loading in one direction did not appear to be influenced by previous loading in the other loading direction. This suggested that cyclic behavior for a limited number of cycles may be uncoupled into two sets of monotonically increasing load components.

5. For wall W2 that was controlled by flexural cracking, shear strains were noticed only in the compression zone. A substantial redistribution of shear strain was observed as the flexural crack propagated across the base towards the toe.

6. Nondestructive estimates of wall shear strength can be more accurate if shear is assumed to be resisted by only the uncracked portion of wall. Thus for cracked walls, the L/h aspect ratio and the amount of vertical compressive stress should be considered when extrapolating NDE measurements of shear stress at a point to give component strength.

In summary, the limited number of test walls suggested that unreinforced masonry walls can be considered as ductile elements capable of dissipating energy through hysteresis. The superior performance of the test walls was attributed to the vertical compressive stress. Lateral strength of a structural system comprised of unreinforced masonry elements may be assumed to be the sum of strengths of all such elements rather than be limited by the strength of the weakest element.

REFERENCES

1. ABK. "Methodology for Mitigation of Seismic Hazards in Existing Unreinforced Masonry Buildings: the Methodology," Technical Report 08, 1984.

2. Abrams, D. P. "Safe Limits for Lateral Capacity of Cracked URM Walls. " *Proceedings of Sixth Canadian Masonry Symposium*, University of Saskatchewan, June 1992.

3. Abrams, D. P. "Strength and Behavior of Unreinforced Masonry Elements," *Proceedings of Tenth World Conference on Earthquake Engineering*, Madrid, Spain, July 1992.

4. Abrams, D. P., "Masonry as a Structural Material," *Proceedings of ASCE Material Congress*, Atlanta, Georgia, August 1992.

5. Abrams, D. P., and G.S. Epperson, "Evaluation of Shear Strength of Unreinforced Brick Walls Based on Nondestructive Measurements," *Proceedings of Fifth Canadian Masonry Symposium*, pp. 817–826, University of British Columbia, June 1989.

6. Abrams, D. P., and W. Xu, "Evaluation of In-Plane Shear Resistance of Cracked. Unreinforced Brick Walls," *Proceedings of the 9th Intentional Brick/Block Masonry Conference*, Vol. 1, pp. 260–267, Berlin, Germany, Oct. 1991.

7. Atkinson, R. H., B.P. Amadei, S. Saeb, and S. Sture, "Response of Masonry Bed Joints in Direct Shear, " *Journal of Structural Engineering*, ASCE. Vol. 115. No. 9. pp. 2276–2296, 1989.

8. *Building Code Requirements for Masonry Structures and Specifications for Masonry Structures*, ACI 530-88/ASCE 5-88.

9. *Commentary on Building Code Requirements for Masonry Structures and Commentary on Specifications for Masonry Structures*, ACI 530-88/ASCE 5-88.

10. *Commentary to Chapter 24, Masonry of the Uniform Building Code*, The Masonry Society, Boulder, Colorado, 1988.

11. Epperson, G. S., and D.P. Abrams, "Nondestructive Evaluation of Masonry Buildings." Advanced Construction Technology Center, Report No. 89-26-03, University of Illinois at Urbana-Champaign, October, 1989.

12. Epperson, G. S., and D.P. Abrams, "Evaluating Lateral Strength of Existing Unreinforced Brick Masonry Piers in the Laboratory," *Proceedings of Fifth North American Masonry Conference*, pp, 735–746, University of Illinois at Urbana-Champaign, June 1990.

13. Kingsley, G. R , and J.L. Noland, "An Overview of Nondestructive Technique for Evaluation Structure Properties of Brick Masonry," *Proceedings of Second Joint US-Italy Workshop*, August 1987.

14. Noland, J.L., G.R. Kingsley, and R.H. Atkinson, "Utilization of Nondestructive Techniques into the Evaluation of Masonry," *Proceedings of the Eighth International Brick and Block Masonry Conference*, Dublin, Ireland, September 1988.

15. Noland, J.L., et. el., "Nondestructive Evaluation of Masonry Structures," Atkinson-Noland and Associates, Boulder, June 1990.

16. Plummer, H.C., and J.A. Blume, "Reinforced Brick Masonry and Lateral Force Design," Structural Clay Products Institute, Washington D.C., 1953.

17. Schneider, R. R., and W.L. Dickey, *Reinforced Masonry Design*, Prentice-Hall, Englewood Cliffs, New Jersey, 1987.

18. Shah, N., and D.P. Abrams, "Design, Construction and Utilization of a Post Tensioned Masonry Laboratory Reaction Structure," *Proceedings of Sixth Canadian Masonry Symposium*, University of Saskatchewan, June, 1992.

19. "Technical Notes on Brick Construction, Technical Note # 35," Brick Institute of America, Reston, August 1989.

20. Appendix Chapter 1 "Seismic Strengthening Provisions for Unreinforced Masonry Bearing Wall Buildings," *Uniform Code for Building Conservation*, June 1990.

APPENDIX A
SHEAR AND VERTICAL STRAIN TEST DATA

A.1 Lateral Force vs. Shear Strain Relations

As noted in Chapters 2 and 4, shear strain was deduced from the series of five sets of diagonal and vertical displacement transducers shown in Fig. A.1. Shear strain was computed using signals from two diagonal and the two adjacent vertical transducers using Eq. 2.1. These shear strains represent an average of the shear strains across the gage length, and are used to plot the distributions shown in Figs. 4.7 and 4.8. On the following pages of this appendix, the measured relations between lateral force and shear strains at individual points (A through E) are given as reference material.
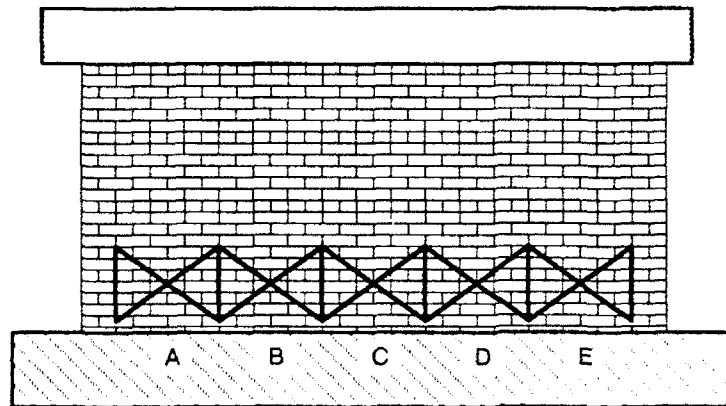
Figure A.1 Shear Distortion Measurement Locations

The excessive values of shear strain for Wall 2 at point A is because a crack passed through the gage length.
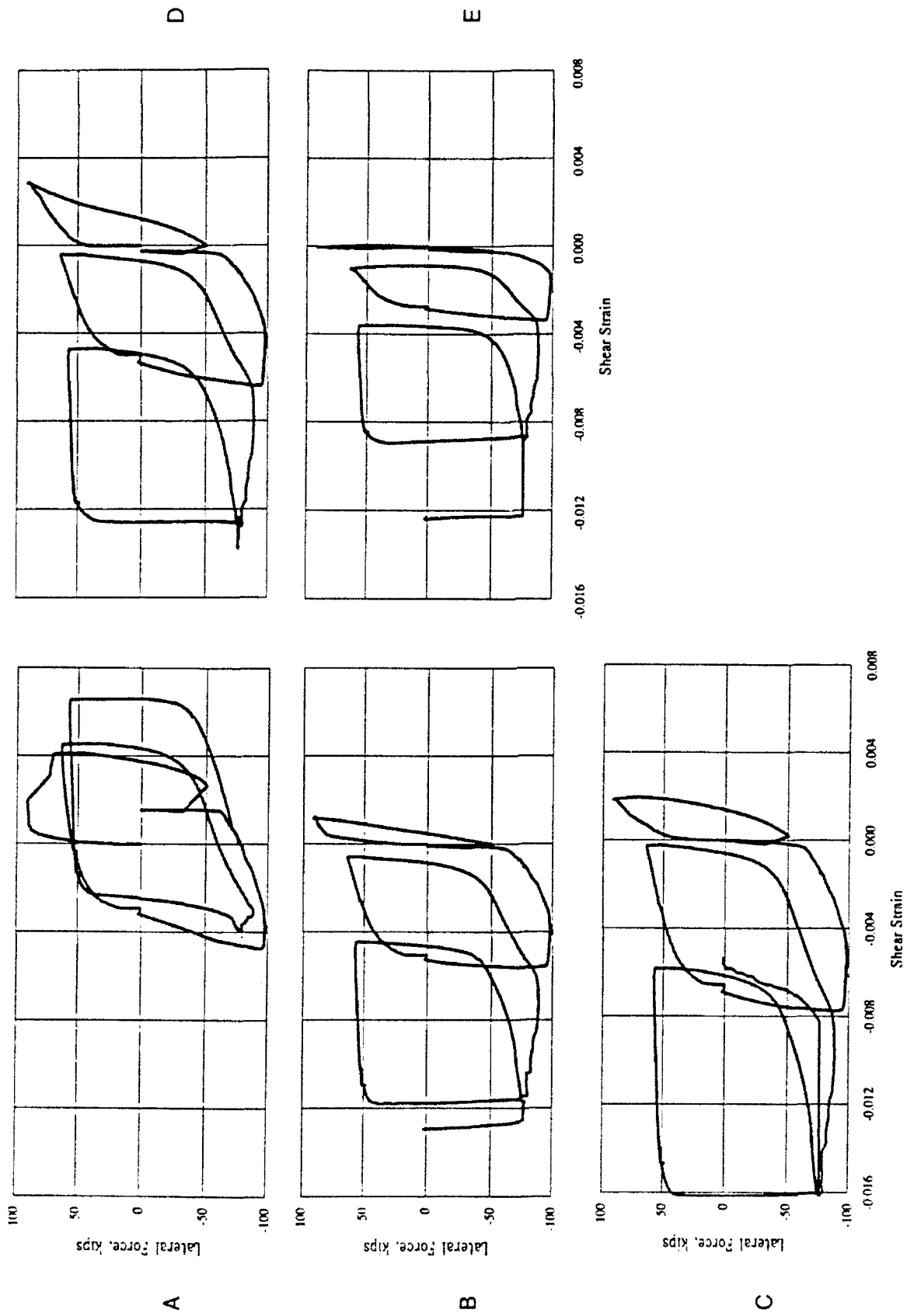
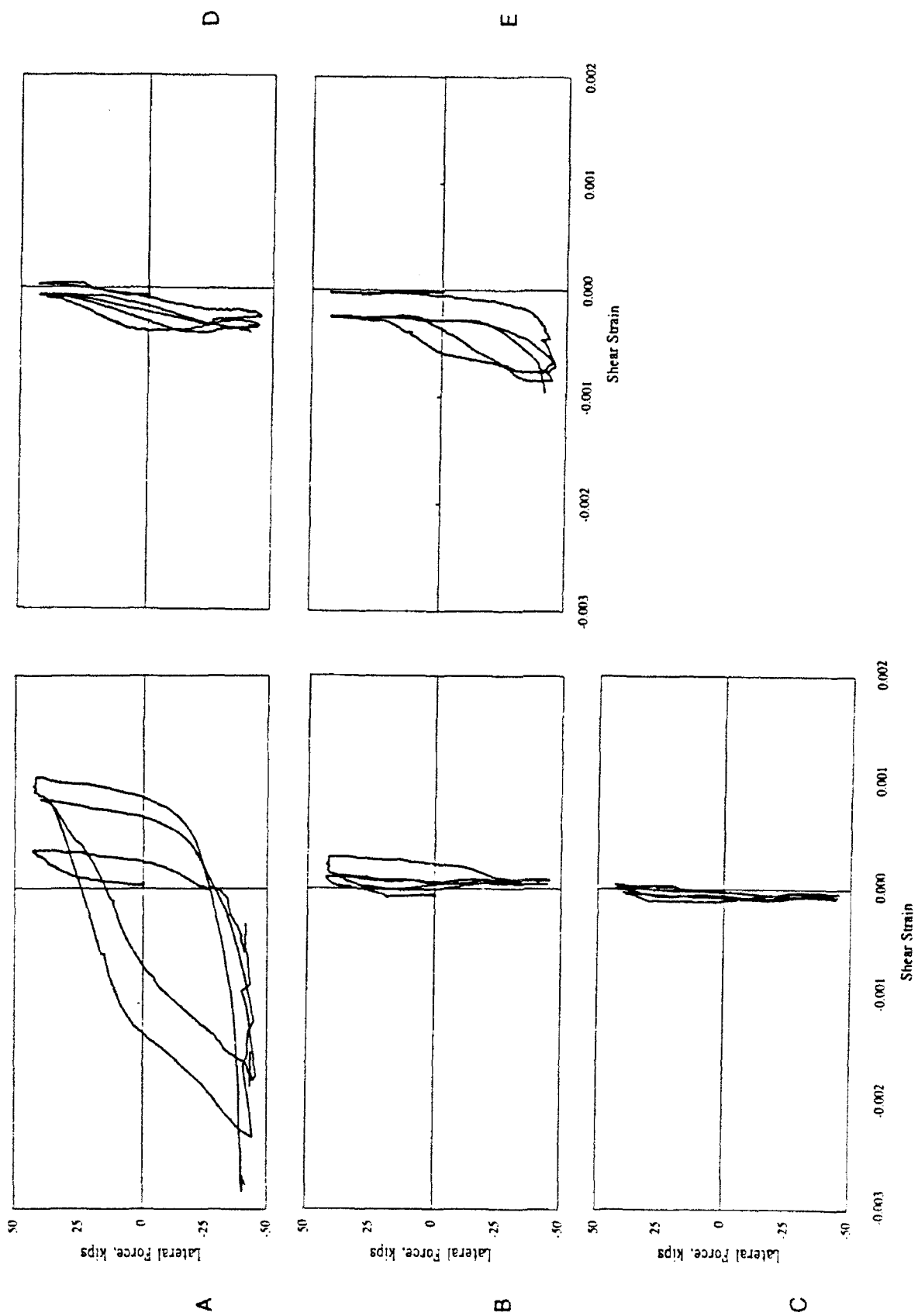Fig. A.2 Measured Relations between Lateral Force and Shear Strain: Specimen W1

40

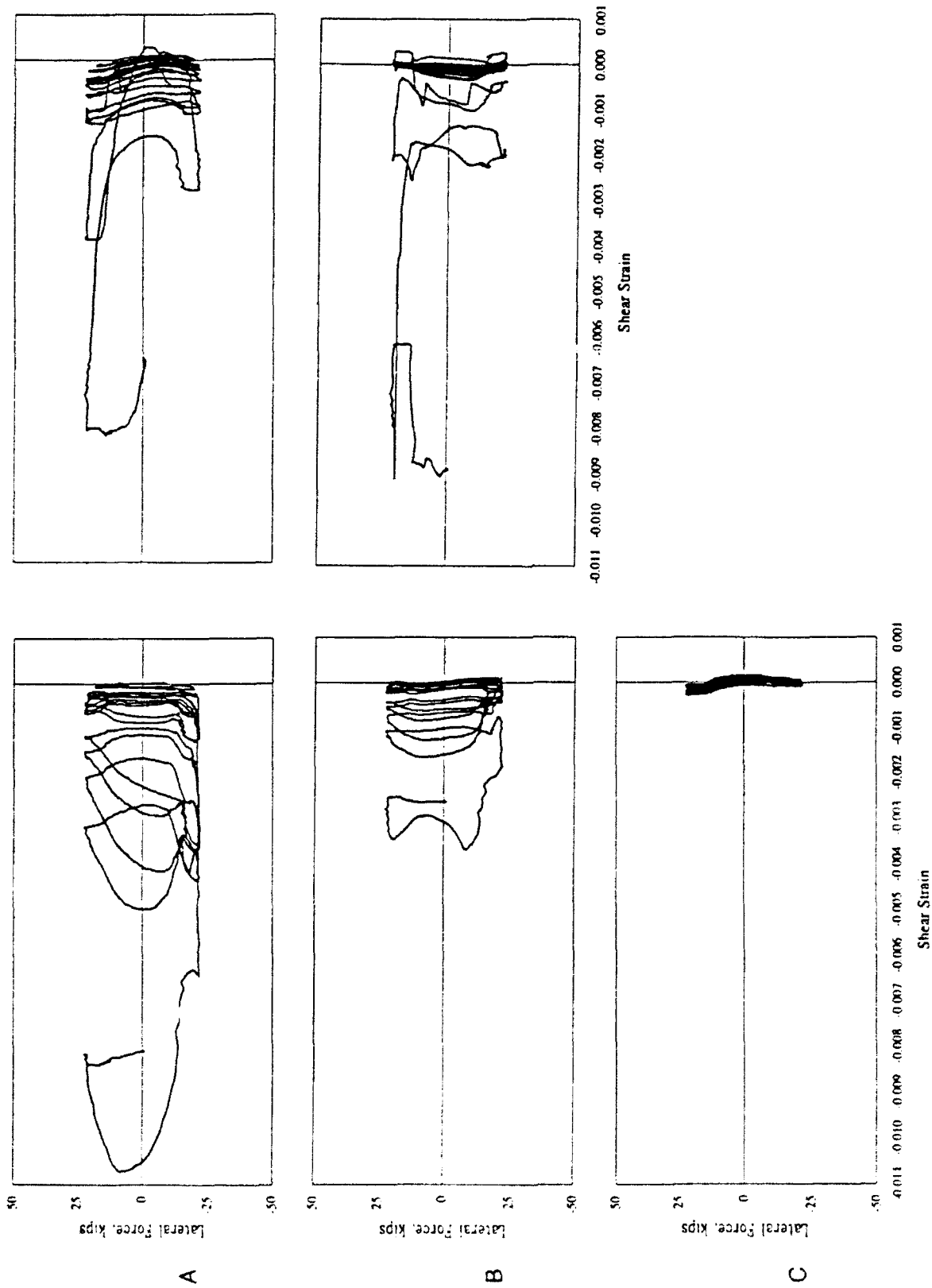Fig. A3 Measured Relations between Lateral Force and Shear Strain: Specimen W2

41

Fig. A.4 Measured Relations between Lateral Force and Shear Strain: Specimen W3

42

A.2 Lateral Force vs. Vertical Strain Relations

As noted in Chapters 2 and 4, vertical strain at six points across the bottom of the wall were measured with displacement transducers. The distribution of vertical strains for various force levels is shown in Fig. 4.10. Vertical strains were deduced from the vertical displacement transducers shown in Fig. A.5. These strains represent an average of the normal strains across the gage length. On the following pages of this appendix, the measured relations between lateral force and vertical strain at individual points (A through F) are given as reference material.
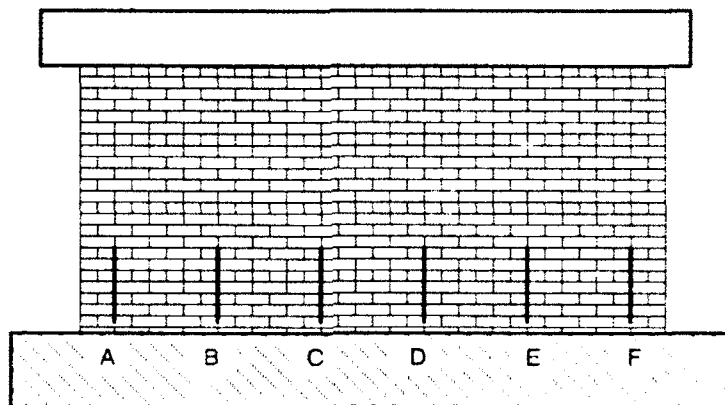

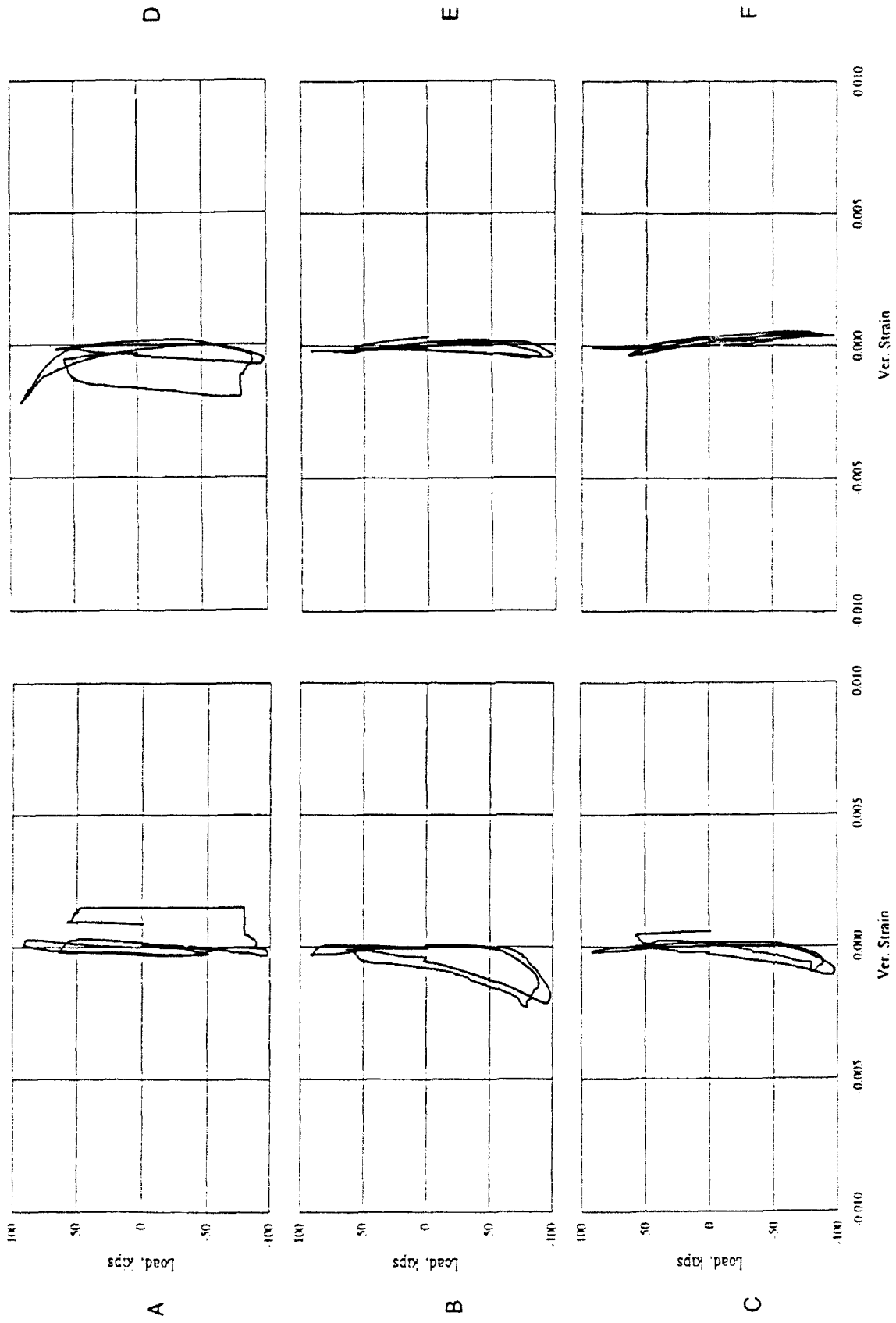
Figure A.5 Vertical Strain Measurement Locations

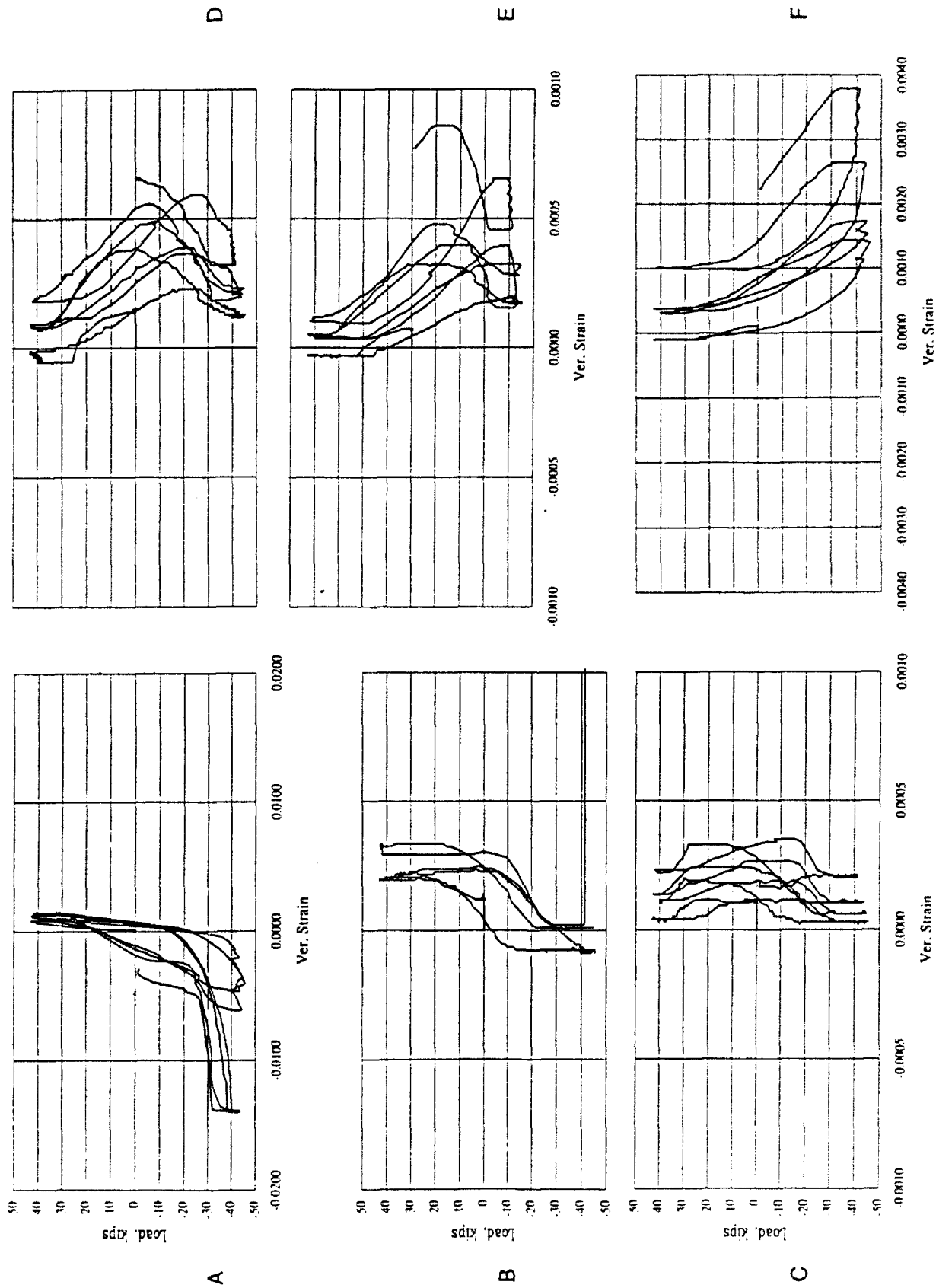Fig. A.6 Measured Relations between Lateral Force and Vertical Strains: Specimen W1

44

Fig. A.7 Measured Relations between Lateral Force and Vertical Strain: Specimen W2
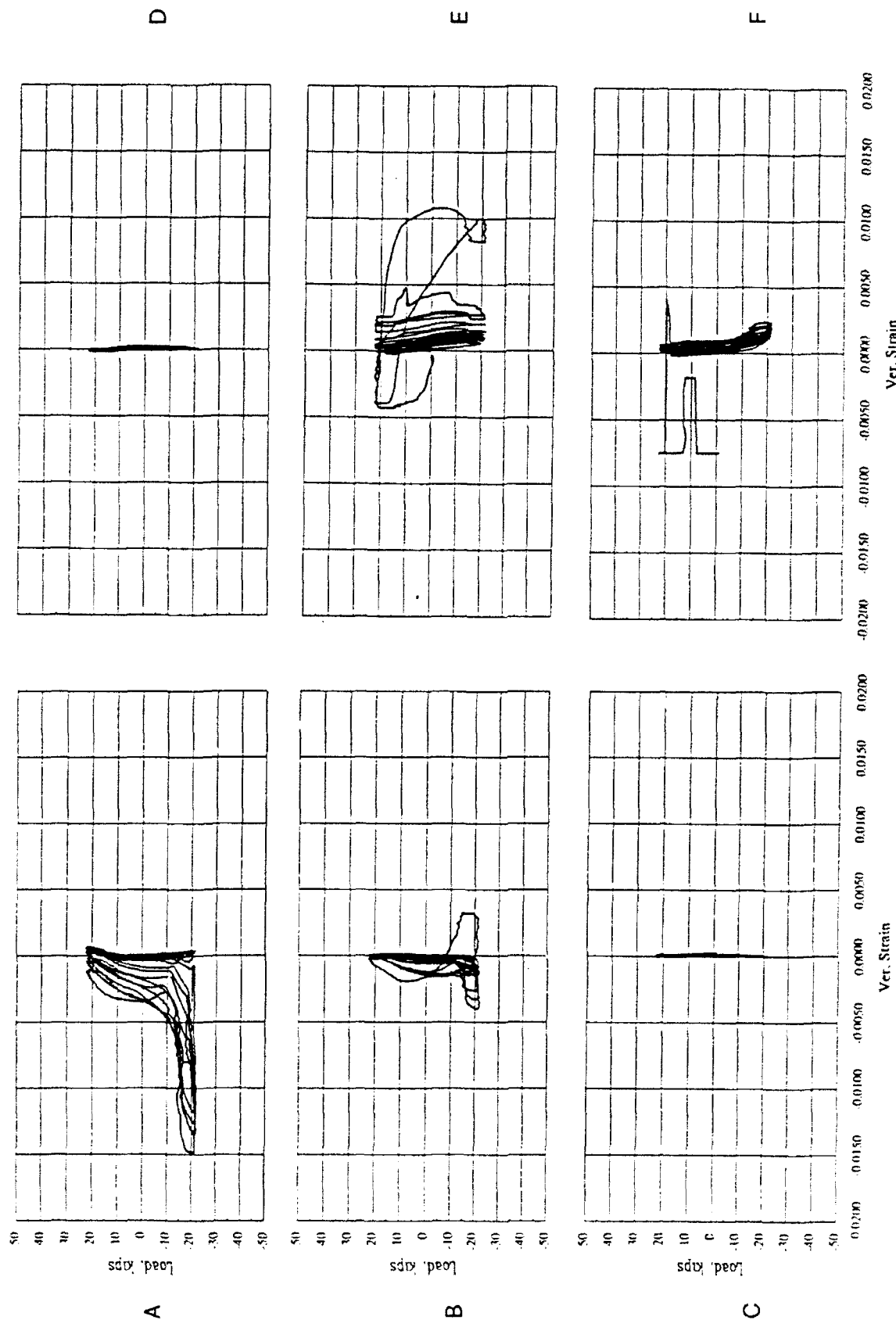
45

Fig. A.8 Measured Relations between Lateral Force and Vertical Strain: Specimen W3